Doctoral Thesis

Identification of Nucleoporin 93 (Nup93) that mediates antiviral innate immune responses

Monwan Warunthorn

Nara Institute of Science and Technology
Graduate School of Biological Sciences
Molecular Immunobiology

(Professor Taro Kawai)

2019/07/29

Contents

Graduate School of Biological Sciences Doctoral Thesis Abstract

Lab name（Supervisor）	Molecular Immunology (Prof. Taro Kawai)		
Name (surname) (given name)	Monwan Warunthorn	Date	(2019/07/29)
Title	Identification of Nucleoporin 93 (Nup93) that mediates antiviral innate immune responses		

Abstract

   Innate immunity is crucially important in host defense from infection of pathogens such as virus and bacteria. Innate immune system is mediated by myeloid cells including macrophages and dendritic cells that recognize pathogen-associated molecular patterns (PAMPs) derived from infectious pathogens by germline-encoded pattern-recognition receptors (PRRs). Recognition of PAMPs by PRRs in these cells triggers innate immune response which produces large amounts of pro-inflammatory cytokines and type I interferons (IFNs). A wide variety of PAMPs including protein, nucleotides, lipid and lipoprotein are recognized by PRRs, including Toll-like receptor (TLRs), Retinoic acid-inducible gene (RIG)-I-like receptors (RLRs), NOD-like receptors (NLRs), C-type lectin receptors (CLRs) and cytosolic DNA sensors such as cGAS. Among them, the RLR family consists of RIG-I and Melanoma differentiation factor 5 (MDA5), which recognize viral RNA. RIG-I detects short double-stranded RNA (dsRNA) with 5′-triphosphate (5′-ppp) or 5′-diphosphate (5′-pp) group and short synthetic dsRNA analogue, polyinosinic:polycytidylic acid (poly(I:C)) whereas MDA5 recognizes long dsRNA and long poly(I:C). Upon RNA recognition, RIG-I and MDA5 recruit an adaptor protein interferon-β promoter stimulator 1 (IPS-1, also known as mitochondrial antiviral signalling, MAVS) for downstream signaling leading to activation of TANK binding kinase-1 (TBK1), which mediates phosphorylation and activation of interferon regulatory factor 3 (IRF3) for type I IFNs and also cytokine expression.

   In this study, I hypothesized that the innate immune genes in invertebrates might have similar functions in mammals. I have searched and identified Nucleoporin 93 (Nup93) as my candidate. Nup93 is one component of nuclear pore complex (NPC) which is composed of a set of approximately 30 different proteins and are evolutionarily conserved from insect to human. Here, I found that Nup93 expression was upregulated after LPS, poly(I:C) and IFN stimulatory DNA (ISD) stimulation, which are agonist for TLR4, RIG-I and cGAS respectively. I generated Nup93-deficient RAW264.7 murine macrophage cell line by CRISPR/cas9 genome editing system. Nup93 deficiency impaired *Ifnb1*, *Il6* and *Cxcl10* expression and production of IFNβ after LPS, poly(I:C) and ISD stimulation. Moreover,

Nup93 deficiency also suppressed *Ifnb1* expression after New castle disease virus (NDV) infection which is sensed by RIG-I. Silencing of Nup93 in primary cells including mouse bone marrow-derived macrophages (BMMs) and murine embryonic fibroblasts (MEFs) showed reduced expression of *Ifnb1* and *Cxcl10* in response to poly(I:C) stimulation. Moreover, exogenous expression of FLAG-Nup93 in Nup93 KO cells restored *Ifnb1* expression following poly(I:C) stimulation. These results suggest that Nup93 regulates type I IFN induction during activation of innate immune signaling pathways.

I then tested phosphorylation and translocation of interferon regulatory factor 3 (IRF3), a key transcription factors for cytokines gene expression, and found that IRF3 phosphorylation and nuclear translocation were impaired in Nup93 KO cells. TBK1 is a protein kinase that phosphorylates IRF3 and causes IRF3 nuclear translocation. I found that TBK1 autophosphorylation was decreased in Nup93 KO cells after poly(I:C) stimulation. IFN-β promoter activity induced by TBK1 overexpression was also increased when co-transfected with Nup93, suggesting that Nup93 facilitates TBK1 activation. Moreover, Nup93 mutant which deleted β sheet at NIC96 domain (591-594aa) failed to enhance IFN-β promoter activity induced by TBK1 and it failed to restored *Ifnb1* expression in Nup93 KO cells. I also found TBK1-Nup93 interaction by pull down and immunoprecipitation, and Nup93 mutant reduced the association with TBK1, suggesting that β sheet at NIC96 domain in Nup93 required for interaction and activation with TBK1.

Taken together, these results suggest that Nup93 plays an important role in antiviral innate immune responses by regulating TBK1. Nup93 is well conserved gene among several species and innate immune response is also one of well conserved host defense system. Therefore, regulatory mechanism by Nup93 may be a conserved mechanism in other species.

1. Introduction

1.1 Innate Immunity

The entry of pathogens into the body triggers activation of host defense system which consists of the acquired and innate immunity. Innate immunity is crucially important in acute response to protect the host from pathogens infection such as virus and bacteria. Innate immune system is mediated by myeloid cells including macrophages and dendritic cells (DCs) that recognize pathogen-associated molecular patterns (PAMPs) derived from pathogens through germline-encoded pattern-recognition receptors (PRRs). Recognition of PAMPs by PRRs in these cells triggers innate immune responses to produce pro-inflammatory cytokines and type I interferons (IFNs). A wide variety of PAMPs such as protein, nucleotides, lipid and lipoprotein are recognized by PRRs including Toll-like receptors (TLRs), Retinoic acid-inducible gene (RIG)-I-like receptors (RLRs), NOD-like receptors (NLRs), C-type lectin receptors (CLRs) and cytosolic DNA sensors such as cyclic GMP-AMP synthase (cGAS). Moreover, innate immunity plays a central role in activating the subsequent adaptive immune response. DCs initiate adaptive immune response by producing cytokines and presenting antigen to T cells. Antigen presented T cells differentiate to helper T cells which help B cells for antibody production and cytotoxic T cells which kill infected target cells. Antigen specific B cells produce antibodies to suppress viral and bacterial growth (Figure 1.1).
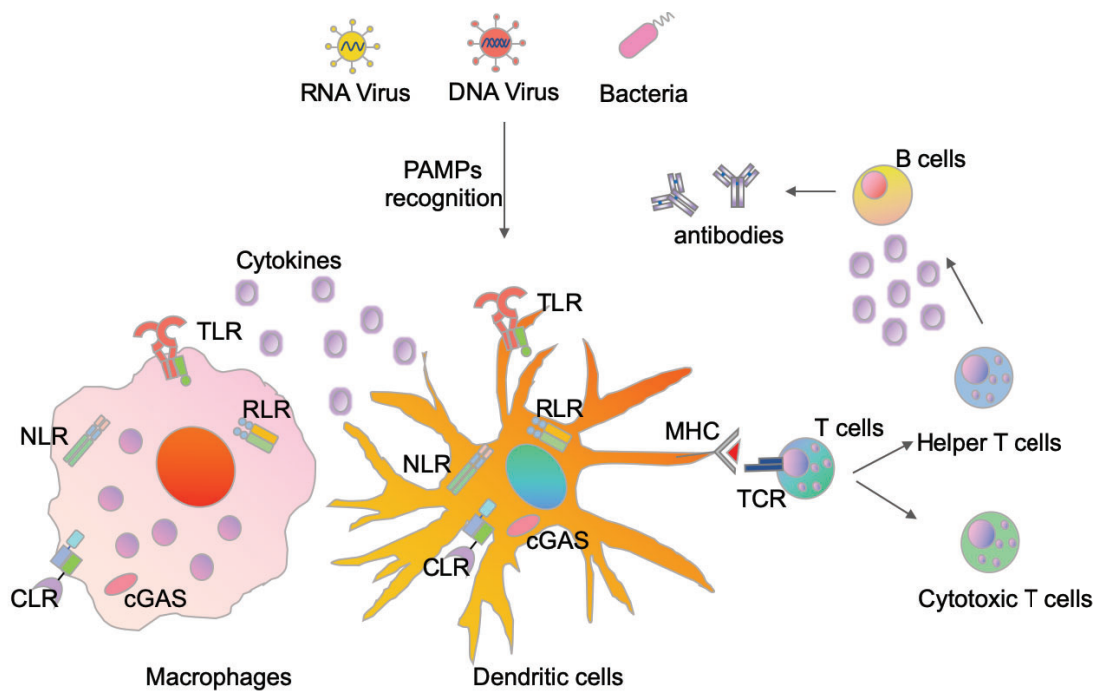
Figure 1.1 Innate immune system activates adaptive immunity. Innate immune system is the first line of host defense system against pathogens infection. Upon infection, myeloid cells including macrophages and dendritic cells recognized pathogens derived PAMPs by PRRs, which trigger production of wide variety of cytokines. PRRs contains TLR, CLR, NLR, RLR and cGAS. PAMPs recognition by these PRRs activates DCs and macrophages which secret cytokines and present antigen. Cytokines and antigen presentation activate T cells for including the adaptive immune response. Helper T cells help B cells for antibody production and cytotoxic T cells kill infected target cells.

1.2 Toll-like receptors (TLRs)

TLR family is a single transmembrane protein that has leucine-rich repeats in ectodomain and cytoplasmic Toll–interleukin 1 (IL-1) receptor (TIR) domain required for signal transduction. TLRs reside within plasma membrane or endosomal membrane compartments. TLR1, TLR2, TLR4, TLR5 and TLR6, which reside on plasma membrane, recognize gram positive bacteria cell wall components, gram negative bacteria cell wall components, lipopolysaccharide (LPS), flagella, respectively (Akira et al., 2006; Kawai and Akira, 2010; Pandey et al., 2015) (Figure 1.2). TLR3, TLR7, TLR9, TLR11, TLR12 and TLR13 localize in intracellular organelles such as endosome and recognize DNA or RNA from bacteria and virus (Barton, 2007; Pandey et al., 2015) (Figure1.2). TLR3 is one of the major

RNA sensors and recognize viral double-stranded RNA (dsRNA) and synthetic analogue of dsRNA polyinosinic-polycytidylic acid (poly(I:C)). TLR7 and TLR8 recognize single-stranded RNA (ssRNA) and viral ssRNA. TLR9 is displayed in endosome and recognize bacterial and viral DNA unmethylated CpG DNA motif. TLR11, TLR12, and TLR13 recognize flagellin, profilin, and bacterial 23sRNA, respectively.

Upon recognition of PAMPs, TLRs recruit adaptor proteins which recruit signaling molecules for activation of transcription factor. TLR4 is firstly identified as PRRs which recognize LPS. LPS-associated TLR4 recruits adaptor proteins such as Myeloid differentiation primary response 88 (MyD88), Toll/IL-1R domain-containing adapter protein (TIRAP), TIR-domain-containing adapter-inducing interferon-β (TRIF) and TRIF-related adapter molecule (TRAM) to form adaptor complex. The adaptor complex then activates several different downstream signaling pathways. MyD88-TIRAP complex recruits and activates serine-threonine protein kinase IL-1R1-associated protein kinases (IRAKs) and interacts with tumor necrosis factor (TNF-α) receptor-associated factor 6 (TRAF6). TRAF6 activates IKK complex (IKKα, IKKβ and NEMO), which phosphorylates IκB molecules. Phosphorylated IκB molecules are degraded by proteasomes and Nuclear Factor kappa-light-chain-enhancer of activated B cells (NF-κB) is liberated and translocates into nucleus and induces proinflammatory gene expression. TRIF-TRAM complex activates another pathway by recruiting TNF receptor-associated factor (TRAF3), which activates TANK binding kinase-1 (TBK1) to phosphorylate interferon regulatory factor 3 (IRF3) for subsequent induction of type I interferons (IFNs) gene expression.
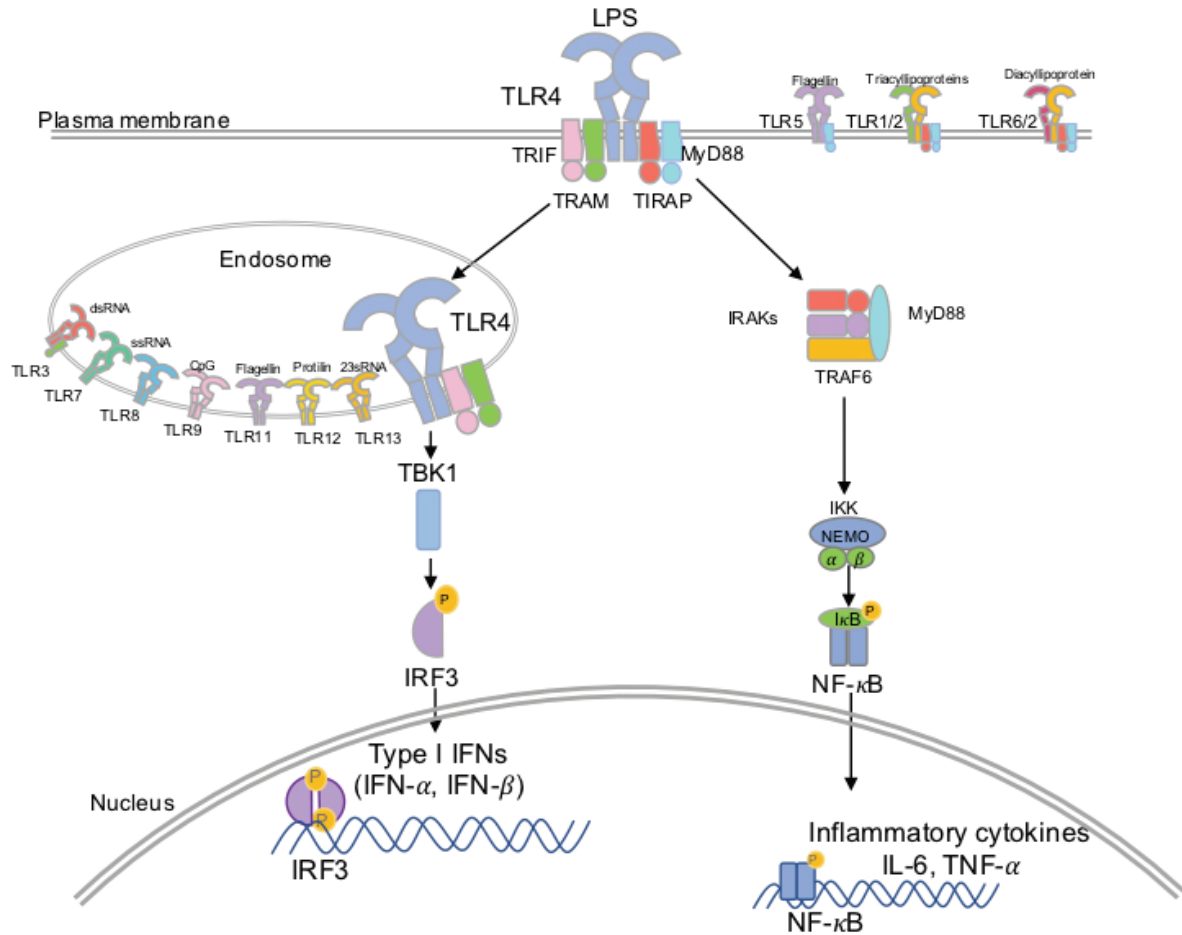
Figure 1.2 Signaling pathway of cell surface and endosomal TLRs. TLR1, TLR2, TLR4, TLR5 and TLR6 localize on the cell surface and recognize LPS, flagellin and the cell wall components of both gram positive and negative bacteria. TLR 3, TLR7, TLR8, TLR9, TLR11, TLR12 and TLR13 localize in the intracellular organelles such as endosome and recognize DNA or RNA from bacteria and virus. TLR4 recognizes LPS by recruiting MyD88 and TIRAP and forming a complex of IRAKs and TRAF6. TRAF6 activates IKK complex, which phosphorylates IκB for NF-κB nuclear translocation. Subsequently, TLR4 translocates to endosomes and recruit TRAM and TRIF, which activate TBK1-mediated phosphorylation of IRF3 for type I IFNs production.

1.3 RIG-I like receptors (RLRs)

RLR family consists of Retinoic acid-inducible gene I (RIG-I) and Melanoma differentiation factor 5 (MDA5), which recognize RNA derived from viral double-stranded RNA in cytoplasm. RLRs expression is strongly induced by IFNs in a positive-feedback loop upon virus detection.

RLRs have a similar helicase core, which comprises two helicase domains, N-terminal caspase recruitment domain (CARDs), a central DEAD box helicase/ATPase domain, and a C-terminal regulatory domain (Figure 1.3). Helicase domains in RIG-I and MDA5 recognize distinct RNA. (Loo and Gale Jr, 2011; Rothenfusser et al., 2005; Saito et al., 2007; Yoneyama and Fujita, 2008). RIG-I recognizes short double-stranded RNA (dsRNA) with 5′-triphosphate (5′-ppp) or 5′-diphosphate (5′-pp) group and short synthetic dsRNA analogue, poly(I:C) whereas MDA5 recognizes long dsRNA and long poly(I:C). RIG-I is required for sensing influenza A virus (IAV), measles virus, Ebola virus, Newcastle disease virus (NDV), Sendai virus (SeV), vesicular stomatitis virus (VSV), and Japanese encephalitis virus (JeV) (Kato et al., 2006; Thompson et al., 2011). In contrast, a class of Picornaviridae including encephalomyocarditis virus (EMCV), Theiler's virus, hepatitis C virus (HCV), mengovirus, and murine norovirus are recognized by MDA-5 (Kato et al., 2006; McCartney et al., 2008). Both RIG-I and MDA5 are able to recognize Dengue virus and West Nile viruses (WNV) (Fredericksen et al., 2008; Gitlin et al., 2006; Loo et al., 2008; Rehwinkel et al., 2010).

Upon activation, RIG-I and MDA5 interact with IFN-β-promoter stimulator 1 (IPS-1, also known as mitochondria antiviral signaling protein MAVS) through homophilic interactions between these N-terminal CARD domains. IPS-1 constitutively localizes on the outer membranes of mitochondria where it interacts with TRAF3 and TRAF6 to form a complex which interacts with the TNFR-associated death domain (TRADD) and Fas-associated protein with death domain (FADD), leading to activation of TBK1 and IKKs, which eventually induce type I IFN and inflammatory cytokines.
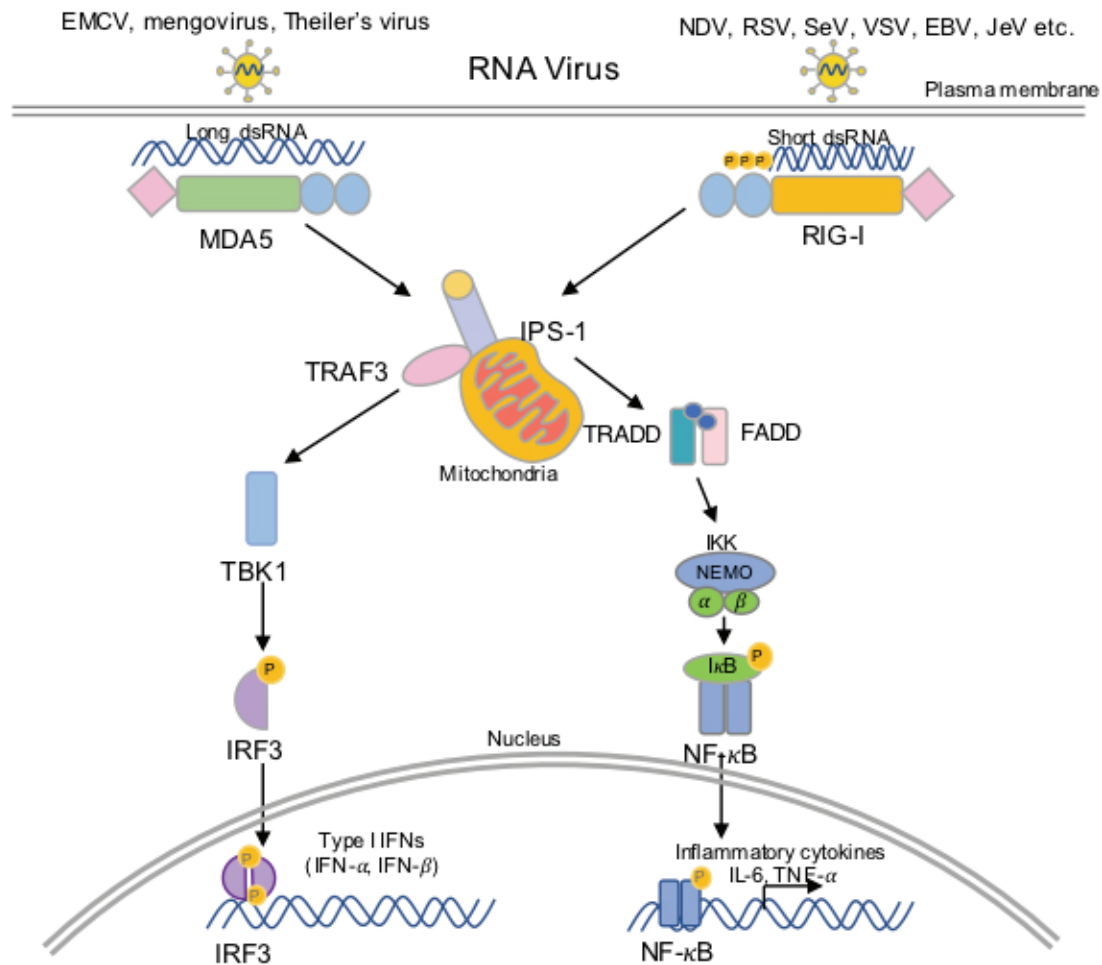
Figure 1.3 RLR signaling pathway RLR family consists of RIG-I and MDA5 which localize in the cytoplasm. RIG-I recognizes short synthetic dsRNA analogue, poly(I:C), Sev, VSV, RSV, NDV, EBV and JEV whereas MDA5 recognizes long poly(I:C), EMCV, Theiler'c virus, HCV, mengovirus and murine norovirus. Upon the infection, RIG-I and MDA5 interact with IPS-1 which localizes in mitochondria. IPS-1 interacts with TRAFs to form a complex with the TRADD and FADD, leading to activation of TBK1 and IKKs for activating type I IFNs and inflammatory cytokines.

1.4 Cytosolic DNA sensor

Cyclic guanosine monophosphate (GMP)-adenosine monophosphate (AMP) synthase or cGAS is an intracellular DNA sensor that localizes in the cytoplasm and recognizes DNA derived from pathogens or host cells (Chen et al., 2016; Dempsey and Bowie, 2015; Li and Chen, 2018; Sok et al., 2018; Sun et al., 2013). cGAS acts as a DNA sensor that produces cyclic GMP-AMP (cGAMP) which is a noncanonical cyclic di-nucleotides (CDN) with unique

phosphodiester linkages between 2′OH of GMP and 5′-phosphate of AMP and between 3′OH of AMP and 5′-phosphate of GMP (Ablasser et al., 2013; Gao et al., 2013; Sun et al., 2013). cGAMP binds to and activates the adapter molecule Stimulator of interferon genes (STING). STING is multi pass transmembrane protein that localizes in Endoplasmic Reticulum (ER). After the complex formation with cGAMP and STING, STING translocates from ER to perinuclear golgi with conformational change and forms a homodimer formation (Ishikawa and Barber, 2008; Saitoh et al., 2009). Then, STING recruits TBK1, which in turn phosphorylates IRF3 and induces nuclear translocation of IRF3 (Liu et al., 2015; Tanaka and Chen, 2012) (Figure 1.4).

cGAS detects and binds to synthetic double-stranded DNA (dsDNA) such as IFN stimulatory DNA (ISD) which is longer than 20 base pairs (Civril et al., 2013; Li et al., 2013). cGAS responds to DNA virus such as human immunodeficiency virus 1 (HIV-1), murine leukemia virus, and simian immunodeficiency virus.
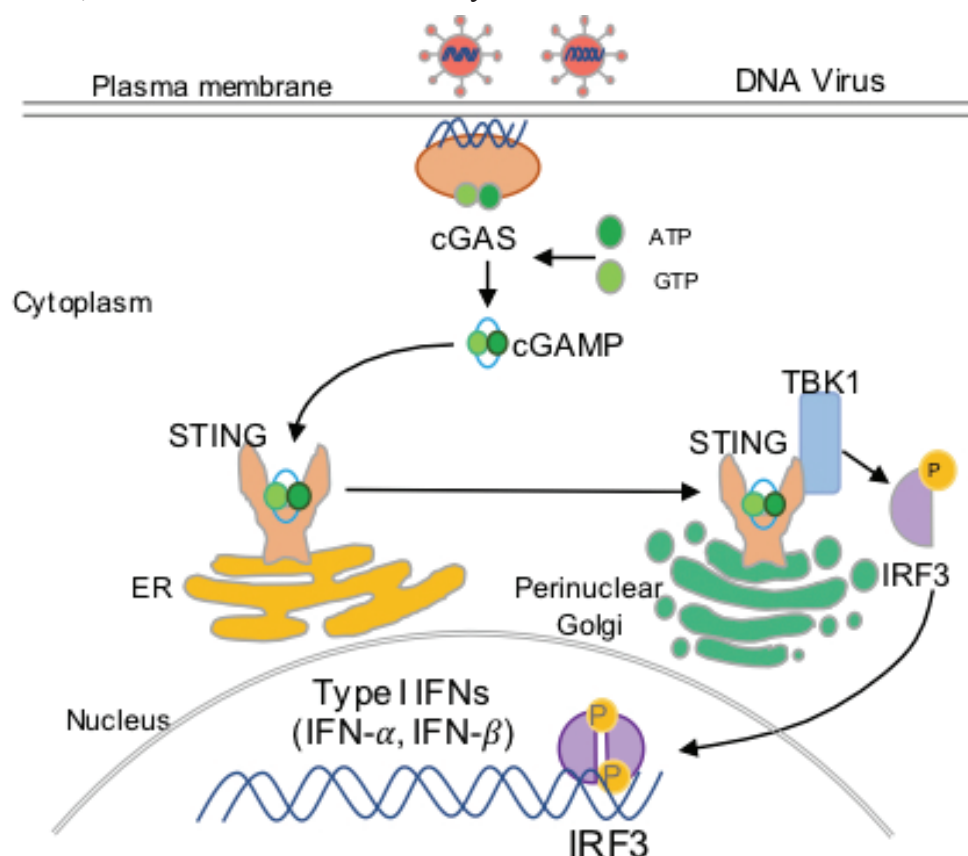

Figure 1.4 cGAS signaling pathway cGAS is a cytosolic DNA sensor that recognizes dsDNA derived from pathogens or host cells. cGAS catalyses the synthesis of cGAMP from GMP and AMP. cGAMP binds to STING, which traffics from ER to perinuclear golgi and recruits TBK1. TBK1 induces phosphorylation and nuclear translocation of IRF3 for type I IFNs production.

1.5 Nucleoporins (Nups)

In eukaryote, nuclear pore complex (NPC) bidirectionally transports essential materials between the nucleus and cytoplasm (Grossman et al., 2012; Li et al., 2016). NPC consists of approximately 30 different types of nucleoporins (Nups) which are involved in the trafficking of macromolecules. The NPC is a modular structure that can be divided into three large regions: the nuclear basket, the central core and the cytoplasmic nuclear filaments. The central core is composed of the outer-ring Nups, inner-ring Nups and center Nups (Hoelz et al., 2011; Le Sage and Mouland, 2013) (Figure 1.5).

Nups are evolutionarily conserved in distant eukaryotes ranging from yeast to human. Several studies have suggested that Nups are involved in the regulation of innate immune signaling pathway in insects and Mammals. Nup98 has been well characterized in innate response in *Drosophila*, which promotes antiviral gene expression to restrict RNA virus infection (Panda et al., 2014). Nup214-Nup88 complex functions in NF-κB translocation and the activation of immune response in *Drosophila* (Xylourgidis et al., 2006). In human, Nup96 was induced by IFNs and involved in antiviral functions (Enninga et al., 2002; Faria et al., 2006).

Nup93 that contains large Nucleoporin-interaction component (NIC) 96 domain (Figure 1.6). Nup93 is shown to be essential for NPC formation and located at inner-ring Nups. N-terminal coiled-coil region in Nup93 is important in the recruitment of Nup62 complex and establishment of the permeability barrier and transport competency of the NPC. C-terminal region of Nup93 is NIC96 domain in which two alpha-helical (α) regions and blinkered by beta-sheet (β) (Sachdev et al., 2012). Nup93 interacts with several nucleoporins including Nup62, Nup58 and Nup54 (Chug et al., 2015). Mutation of Nup93 at the amino acids position Lysine442, Glycine591 and Tyrosine629 was reported to cause NPC dysfunction and steroid-resistant nephrotic syndrome (SRNS) by abrogating interaction with Importin7 (Braun et al., 2016; Hashimoto et al., 2019). Previous reports suggested that Nup93 interacts with other NPC such as Expotin1 (XPO1) which regulates antiviral immune response through DExD box RNA helicase (DDX3) (Baril et al., 2013; Yedavalli et al., 2004) although the mechanism that regulated DDX3-induced antiviral immunity is uncertain. Here, I generated Nup93 deficient murine macrophage cell line and found that Nup93 plays important roles in RLR-mediated innate immune response by facilitating TBK1 activity.
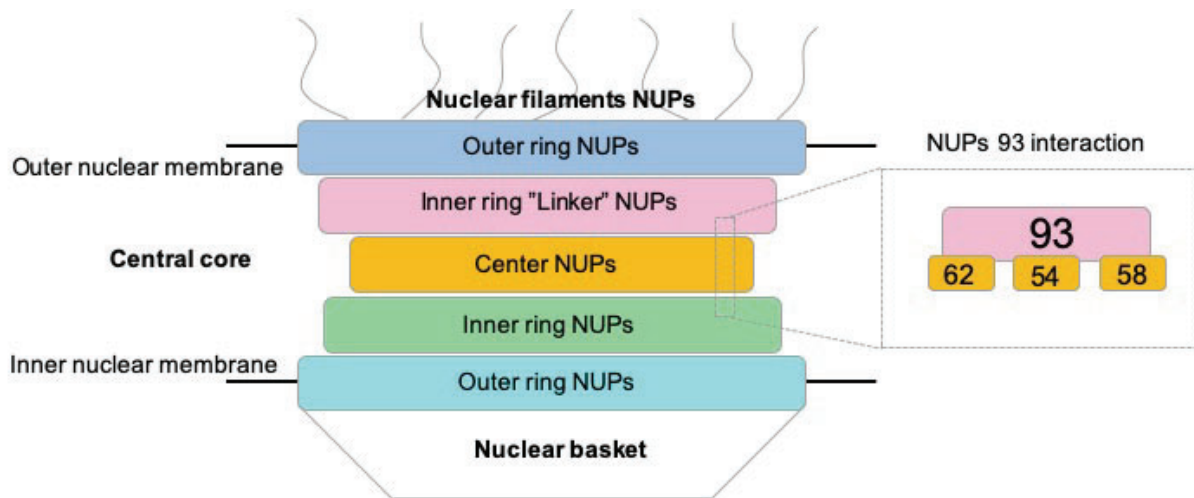
Figure 1.5 Structure and molecular composition of the nuclear pore complexes (NPCs)
NPCs divided into several groups according to their location and structural characteristics. The central core is composed outer-ring Nups, inner-ring Nups or linker Nups and center Nups. Asymmetric Nups structure is composed the nuclear basket and the cytoplasmic filaments. Nup93 locates at Inner-ring or linker-Nup at the central core and interacts with Nup62, Nup54 and Nup58.

Figure 1.6 A schematic domain of Nup93 Nup93 consists of nucleoporin interaction component. The N-terminal coiled-coil region is marked in yellow, the two alpha-helical regions are marked in purple and blinkered beta-sheet is marked in pink.

2. Materials and Methods

2.1 Mice

Wild-type C57BL/6 (6–10 weeks of age) mice were obtained from CLEA Japan. All animal maintenance and experiments were accordance with the guidelines of the Committee on Animal Research at Nara Institute of Science and Technology (NAIST).

2.2 Cells

RAW264.7 (mouse murine macrophage cell line) cells, Human Embryonic Kidney 293 (HEK293) cells, HEK293T cells and Mouse Embryonic Fibroblasts (MEFs) cells were cultured in Dulbecco's modified Eagle's medium (DMEM, Nacalai Tesque) supplemented with 10% heat-inactivated fetal bovine serum (FBS, Thermo Fisher Scientific) in 5% CO_2-humidified incubator (Life technologies). D-Phosphate Buffer Saline (D-PBS, Nacalai Tesque), 10mM Ethylene diaminetetraacetic acid (EDTA, Nacalai Tesque) in 2.5 mg/l trypsin (Nacalai Tesque) were used for washing and dissociating adherent cells respectively.

Mouse bone marrow-derived macrophages (BMMs) were differentiated from mouse bone marrow cells in Roswell Park Memorial Institute medium 1640 (RPMI 1640, Nacalai Tesque) containing 10% FBS, 100 units/ml penicillin 100 µg/ml streptomycin (Nacalai Tesque), 100 µM of β-mercaptoethanol (Nacalai Tesque) and 20 ng/ml of murine macrophage colony-stimulating factor (M-CSF) (BioLegend) in a 5% CO_2-humidified incubator. BMMs were harvested at day 7 using D-PBS with 10 mM EDTA and subjected to subsequent experiments.

2.3 Reagents

Lipopolysaccharide (LPS) and High molecular weight Polyinosinic-polycytidylic acid (HMW poly(I:C)) were purchased from InvivoGen. Sense and anti-sense IFN stimulatory DNA (ISD) sequences were synthesized by Eurofin Genomics and annealed manually (5′-TACAGATCTAC TAGTGATCTATGACTGATCTGTACATGATCTACA-3′). Poly(I:C) and ISD were each mixed with Lipofectamine 2000 (Life Technologies) a ratio 1:1 (µg/µl) in Opti-MEM (Life technologies) for intracellular stimulation. Newcastle Disease Virus (NDV) was provided according to publication of (Kawai et al., 2005).

Table 2.1 Ligands, their cognate PRRs and concentration

PRR	Ligand/Virus	Concentration
TL4	LPS	100 ng – 1 µg /ml
MDA5	poly(I:C)	1 µg/ml
RIG-I	NDV	MOI=10
cGAS	ISD	1 µg /ml

2.4 Plasmids

Full-length of Nup93, Nup93Δwere amplified by PCR from cDNA mouse testis tissue and inserted to pFlag-CMV™-2 expression vector (Sigma) or pMRX-vector.

Table 2.2 List of primers

Name	Sequence (5'-3')	Target
Nup93_EcoRI_F	AAGAATTCTAAAATGGACTACAAAGACGATGAC	Clone
Nup93_BamHI_R	ATAGAATTCTTAATTCATGAGGACCTCCATC	Clone
pCAG_BamHINup93-F	ATAGAATTCCATTTGTTTTACCATGGCCCA	Clone
pCAG_EcoRINup93-R	AATAGAATTCGTGTCCACTCACAATCTTCTC	Clone
px330_Nup93-F	CACCTGTAAATTTCGTTCTACATG	Clone
px330_Nup93-R	AAACCATGTAGAACGAAATTTACA	Clone
Nup93_G_F_Exon4	CAGAAAGTGAAGGTTTTCCAGTCA	RT-qPCR
Nup93_G_R_exon4	GTGAAATCTGTACTCAGAAACAAAATT	RT-qPCR
mIfnb1_F	ATGGTGGTCCGAGCAGAGAT	RT-qPCR
mIfnb1_R	CCACCACTCATTCTGAGGCA	RT-qPCR
mIl6_F	GTAGCTATAGTACTCCAGAAGAC	RT-qPCR
mIl6_R	ACGATGATGCACTTGCAGAA	RT-qPCR
mTnfa_F	CACAGAAAGCATGATCCGCGACGT	RT-qPCR
mTnfa_R	CGGCAGAGAGGAGGTTGACTTTCT	RT-qPCR
mCxcl10_F	CCTGCAGGATGATGGTCAAG	RT-qPCR
mCxcl10_R	GAATTCTTGTTCGGCAGTT	RT-qPCR
mGapdh_F	TGACGTGCCGCCTGGAGAAA	RT-qPCR
mGapdh_R	AGTGTAGCCCAAGATGCCCTTCAG	RT-qPCR
pMRX_BamHI_Nup93_F	AATGGATCCGCCATGGCCATGGATACTGAGGGGTTTGGTGAG	Clone
pMRX_EcoRI_Nup93_R	GATCAAGCTTGAATTCTTAATTCATGAGGACCTCCATCTGCAC	Clone
Nup93_del1_R	CTGATGCAGATTCACAAGGGTGTA	Clone
Nup93_del2_F	CTAGAGAACGATAAGCCTGGAGTTATA	Clone

2.5 Antibodies

Table 2.3 List of antibodies

Antibodies	Company	Concentration
Mouse-anti-FLAG monoclonal antibody	Sigma	1/1,000
Mouse-anti-GST monoclonal antibody	Santa Cruz	1/1,000
Rabbit-anti-Nup93 polyclonal antibody	Sigma	1/1,000
Mouse-anti-Actin monoclonal antibody	Santa Cruz	1/1,000
Rabbit-anti-IRF3 monoclonal antibody (D83B9)	Cell Signaling Technology	1/1,000
Rabbit-anti-phospho-IRF3 monoclonal antibody (4D4G)	Cell Signaling Technology	1/1,000
Rabbit-anti-NAK(TBK1) monoclonal antibody (EP611Y)	Abcam	1/1,000
Rabbit-anti-phospho-TBK1 monoclonal antibody	Cell Signaling Technology	1/1,000
HRP-conjugated anti-mouse IgG monoclonal antibody	Sigma	1/10,000
HRP-conjugated anti-rabbit IgG monoclonal antibody	Sigma	1/10,000
Alexa Fluoro488 Goat anti-Rabbit IgG (H+L)	Invitrogen	1/10,000
Alexa Fluoro568 Goat anti-Mouse IgG (H+L)	Invitrogen	1/10,000

2.6 RT-qPCR

RAW264.7 and BMMs at 3×10^5 cells/ well in 24 well plates (Corning) were stimulated with 1 μg/ml of LPS for 2 hours (h), 1 μg/ml poly(I:C), and 1 μg/ml ISD for 6 h. Stimulations were stopped by administration of Tri reagent (MRC).

2.6.1 Total RNA extraction and first strand cDNA synthesis

Total RNA was extracted by Tri reagent according to the manufacturer's protocol. Briefly, cells in 24 wells plate were applied 500 μl of Tri reagents and were transferred into micro tube. Samples were added 100 μl of chloroform were incubated on ice 30 m. Samples were centrifuged at 13,000 rpm for 15 m 4 ˚C. Upper phase of solutions were transferred to new tube and RNAs were precipitated with 1 volume of isopropanol. Then, the sample was centrifuged at 13,000 rpm for 15 m at 4˚C. Pellets were collected and were washed with 75 % ethanol. RNA pellets were air-dried and were dissolved with Diethyl pyrocarbonate (DEPC) water. Then, total RNA was measured by nanodrop (Thermo scientific) at A_{260}/A_{280}. First-strand cDNA was synthesized using ReverTra Ace Synthesis kit (Toyobo). Mixtures were incubated at temperature in a series of 30˚C for 10 m, 42˚C for 60 m and 70˚C for 10 m, respectively, and were stored at -20˚C refrigerator for further investigation.

2.6.2 Quantitative real-time RT-PCR

Real-time RT-PCR analysis was performed with Power up sybergreen Supermix (Applied Biosystem). The amplification was performed in PCR white plate in a 20 μl reaction volume containing 10 μl of Power up sybergreen supermix (Applied Biosystem), 2 μl of each qPCR-Nup93 F/R primers (10 mM), and 3 μl of 1:10 diluted cDNA template (Table 2.2). The reactions were detected by LightCycler 96 (Roche) and were performed with 95°C for 8 m followed by 40 cycles of denaturation (95°C for 30 s), annealing and extension (60°C for 60 s). Specificity of primers was verified by measuring the melting curve of the PCR product at the end of the reaction. The relative quantification was calculated the amount of target transcript relative to an internal standard, mGapdh F/R primer. A mathematical model was used to determine the relative expression ratio (Pfaffl, 2001).

$$\text{Real expression ratio} = (E_{target})^{\Delta ct\ target\ (control-sample)} / (E_{ref})^{\Delta ct\ ref\ (control-sample)}$$

2.7 Generation of Nup93 knockout RAW264.7 cells

2.7.1 Amplification of mouse *Nup93* gene

Gene specific primers of full-length Nup93 (Nup93_EcoRI_F and Nup93_BamHI_R primer) (Table 2.1) were designed from coding sequence of *M. musculus* (accession number NM_172410). Nup93 gene was amplified using a pair of primers contained 5′ flanking EcoRI restriction sites and 3′flanking BamHI restriction site. PCR reaction were performed 50 μl amplification reaction with 2X KOD Fx reaction buffer (Toyobo), 2 mM dNTP, 10 μM each primer, 1 μl cDNA Testis sample and 1 U KOD Fx DNA Polymerase (Toyobo). PCR thermal cycling conditions were 94°C for 3 m, 30 cycles of 98°C for 10 s, 55 °C for 1 m and 68°C for 1 m, and then a final extension at 68°C 10 m.

2.7.2 Preparation of pX330 plasmid

pX330 plasmids contained Cas9 nuclease expression cassette with gRNA expressing promoter. gRNA for genome editing were designed by using chop-chop software (https://chopchop.rc.fas.harvard.edu/). Primers encoding gRNA were conjugated sticky ends of BbsI (Table 2.2). Primer were annealed and kinased by T 4 Kinase Buffer (New England Biolabs). The annealing reaction condition is 95°C for 5 m, primer Tm value + 5°C for 30 m, primer Tm value for 30 m and primer Tm value -5°C for 30 m. After that, the annealing product

was ligated into pX330 treated with the restriction enzyme BbsI (Thermo Scientific) according to the manufacturer instruction.

2.7.3 Preparation of pCAG-EgxxFP plasmid

Gene specific primers were designed from database sequence and were added restriction site BamHI and EcoRI (Table 2.2). DNA fragment 600 bp of Nup93 was amplified by PCR (2× KOD Fx reaction buffer (Toyobo), 2 mM dNTP, 10 μM each primer, 1 μl cDNA Testis sample and 1 U KOD Fx DNA Polymerase (Toyobo)). PCR thermal cycling conditions were 94°C for 3 m, 30 cycles of 98°C for 10 s, 55 °C for 1 m and 68°C for 1 m, and then a final extension at 68°C 10 m. pCAG-EgxxFP and PCR product were double digested with BamHI and EcoRI restriction enzymes (Toyobo).

2.7.4 Ligation

Restriction enzyme digested pX330 and pCAG-EgxxFP were purified with illustraTM GFX ™ PCR DNA and Gel Band Purification kit, PCR DNA fragments were ligated with plasmids with 1:3 ratio and were incubated with 2× Ligation Mix (Nippon Genetics) at 16°C for 2 h.

2.7.5 Transformation

30 μl of competent *E. coli* strain (DH5-α) was melted on ice and was added to the ligation reaction solution. Samples were heat-shocked for 1 m at 42°C and were applied 500 μl of LB liquid medium. Sample were gently mixed and were cultured at 37°C for 1 h. The culture solution was plated to LB plate medium containing 100 μg/ml ampicillin (Nacalai) and LB plates were incubated at 37°C for overnight.

2.7.6 Plasmid extraction and sequencing analysis

Colonized *E. coli* was inoculated into 2 ml of LB broth containing 100 μg/ml ampicillin and were cultured for overnight at 37°C. The culture broth was centrifuged and plasmid purification were carried out according to Fast Gene Plasmid Mini Kit (Nippon Genetics). Concentration of plasmid was measured by Nano drop. Plasmids concentration 100-200 ng was used as a template for the sequence reaction. Sequence reactions were prepared by according to BigDye Terminator v3.1 Cycle Sequencing Kit (Abi). After data collection, nucleotide sequencing was analysed by GENETYX Ver.12 (GENETYX) software and BLAST

(https://blast.ncbi.nlm.nih.gov/Blast.cgi). High-concentration expression plasmid was purified from 50 ml of LB liquid cultures by according to NucleoBond Xtra Midi kit (Takara).

2.7.7 Acquisition of EGFP positive cells derived from 1 cell by FACS Sorting

Recombinant plasmids of pX330 and pCAGExxFP were co-transfected into RAW264.7 cells. Number of RAW264.7 cells were counted to 1.0×10^7 cells/100 μl and transfected 4 μg of each plasmid by electroporation according to the Neon Transfection System (Life Technologies) with 1680 mA, 20 ms, 1 pulse. RAW264.7 cells were incubated for 48 h and were subjected to cell sorting FACS Aria. Briefly, after removal of medium, cells were washed with PBS (Nacalai) and were added 500 μl of FACS Buffer [1% BSA (Sigma), 2 mM EDTA (Nacalai) in PBS]. EGFP-positive cells were detected by FACS Aria (BD Bioscience), and were sorted into a 96 wells plate. Sorted cells were cultured for 2 weeks for genomic sequence.

2.7.8 Determination of mutation position by genomic sequence

RAW264.7 cells isolated by FACS sorting were transferred to 24 wells plate and cultured until cell density reached 70-80%. Cells were added 50 mM NaOH (Wako), incubated at 95°C for 1 h, and neutralized with 1 M Tris-HCl (pH 8.0, Nacalai). PCR was carried out with Ex Taq HS (TaKaRa) using genomic DNA as a template (Table 2.2). PCR reaction conditions were as follows: 98°C for 5 m, 40 cycles of 98°C for 30 s, 55°C for 30 s and 72°C for 1 m. PCR products were analysed by using 1.5 % agarose gel electrophoresis. Expected bands were isolated from agarose gel and DNA were purified by illustra™GFX™PCR DNA and Gel Band Purification kit (GE Healthcare). Target bands were ligated into pMDV-20 TA cloning vector and inserts were checked by blue white screening using 5-bromo-4-chloro-3-indolyl-b-D-galactopyranoside (X-gal). Positive plasmids were sequenced using primers shown in Table 2.2.

2.7.9 SDS-PAGE

Cells in 6 wells plate were lysed by 300 μl of RIPA buffer [0.5% Deoxycholate (Nacalai), 1% NP- 40 (Nacalai), 150 mM NaCI (Nacalai), 0.1% SDS (Nacalai), 50 mM Tris-HCl (Nacalai) pH 8.0] or Lysis buffer [50 mM Tris-HCl pH 8.0, 150 mM NaCl, 5mM EDTA, 1% NP-40] or Homo buffer [150 mM NaCl, 5 mM EDTA, 25 mM Tris-HCl pH 8.0, 0.2% Triton-X-100]. Each protein extraction samples were mixed with SDS sample buffer [0.125 M

Tris-HCl, 4% SDS, 20% Glycerol (Nacalai), 0.01% BPB (Nacalai), 0.2 M DTT (Nacalai)] and these were incubated at 95°C for 5 m. Acrylamide gel were generated using TGX™ FastCast™ Acrylamide kit 12% (BIO-RAD) and samples were run on SDS -PAGE with 20 mA in SDS-PAGE running buffer [0.25 M Tris, 1% SDS, 1.92 M Glycine (Nacalai)].

2.7.10 Western blot analysis

Proteins separated by SDS-PAGE were transferred to Immobilon®-P transfer membrane (Merck Millipore) at 200 mA for 80 m using Transfer buffer [25 mM Tris, 20 % Methanol (Nacalai), 1.92 mM Glycine (Nacalai)]. Membrane was blocked by incubating with 5 % skim milk (Nacalai) for 1 h shake at room temperature. Membrane was incubated with primary antibodies diluted in TBST buffer [0.5 M Tris, 1.38 M NaCl, 0.027 M KCl (Nacalai), 0.05% tween 20 (Nacalai)] with 5 % BSA (Nacalai) at 4°C. After washing with TBST buffer containing 2 % skim milk, membrane was shaken at room temperature for 30 m. After washing, membrane was detected with a luminescent reagent Western Lightning Plus-ECL (PerkinElmer) Enhanced Luminol Reagent and Oxidizing Reagent, and luminescence was detected with Image Quant LAS-4000 (GE Healthcare).

2.8 Expression of *Ifnb1*, *Il6*, *Cxcl10* and *Tnfa* mRNA by LPS, poly(I:C), ISD and NDV stimulation

RAW264.7 3×10^5 cells/well were cultured in 24 wells plate and were stimulated with LPS for 2 h and poly(I:C), ISD, and 10 multiplicity of infection (MOI). NDV for 6 h by following the concentration in Table 2.1. RNA extraction, cDNA synthesis and RT-qPCR were performed. The amount of transcription of *Ifnb1*, *Il 6*, *Cxcl10* and *Tnfa* were quantified by RT-qPCR as describe before. Primers for *Ifnb1*, *Il6*, *Cxcl10*, *Tnfa* and *Gapdh* are shown in Table 2.2. The cytokine expression level was calculated by the ΔΔCt method.

2.9 Measurement of IFN-β, CXCL10 and TNF-α by ELISA

Production of IFN-β, CXCL10 and TNF-α in the cell supernatant was measured by ELISA (enzyme-linked immunosorbent assay). RAW264.7 5×10^4 cells/well were cultured in 96 wells plate and were stimulated by LPS, poly(I:C), and ISD for 24 h by following the concentration in Table 2.1. After each synthetic ligand stimulation, the amount of IFN-β was measured by LumiKine™ m IFN-β (InvivoGen), CXCL10 and TNF-α production were measured using a mouse DuoSet ELISA Development Kit (R & D).

First, 50 µl/well of capture antibody diluted with PBS was added to a 96 wells ELISA plate and were incubated for overnight. After washing with ELISA Wash Buffer [PBS containing 0.05 % Tween 20], PBS containing 1% BSA was added at 300 µl/well and blocking was carried out for 1 h. After washing with ELISA Wash Buffer, 50 µl/well of sample supernatants and control sample for calibration curve were added to ELISA plate and were incubated foe 2 h. After washing with ELISA Wash Buffer, the detection antibody was diluted with 1 % BSA-containing PBS was added at 50 µl/well and were incubated for 2 h. After washing with ELISA Wash Buffer, Streptavidin-HRP diluted 200 times with PBS containing 1 % BSA was incubated for 30 m. After washing ELISA Wash Buffer, plates were added 50 µl/well of Staining solution and Substrate solution in ELISA POD Substrate TMB kit (Nacalai). Then, reaction was stopped with 25 µl of 1 M Sulfuric acid (Nacalai). The absorbance at 450 nm was measured by using an iMARK microplate reader (BIO-RAD), and the amount of protein contained in each sample supernatant was calculated using a calibration curve of standard solutions.

2.10 Nup93 expression by retro virus infection

2.11.1 Preparation plasmid pMRX-FLAG-tagged Nup93

Gene specific primers (pMRX_BamHI_F and pMRX_EcoRI_R) (Table 2.2) were amplified and DNA fragments were cloned to pMRX-IRES-puro vector. The construction of pMRX-FLAG-tagged-Nup93 was used the same condition as describe above.

2.11.2 Retro virus infection

pMRX-FLAG-tagged Nup93 6 µg and pVSV-G 1 µg were co-transfected into Platinum-E cells [Plat E medium: DMEM, 10 % FBS, 1µg/ml puromycin, 10 µg/ml blasticidin] with Lipofectamine 2000 (Life Technologies) in Opti-MEM medium at ratio 1:2 (µg/µl). After transfection, cells were added 10 % FBS and were cultured for 24-48 h. Supernatants were collected and filtered through 0.22 µm Millex-GV Filter (Millipore) with 10 ml syringe (TERUMO). Medium was added polybrene (InvivoGen) and was transferred to Nup93 KO cells or RAW264.7 cells. At the next day, cells were applied with 4 µg/ml puromycin. Surviving cells were used for RT-qPCR and Western Blot (WB) experiments.

2.11 Nup93 knockdown

Knockdown was performed with siRNAs electroporation (Table 2.4). BMMs and MEFs 1×10^6 cells/ 100 µl were electroporated with 3 µM siRNA by Neon Transfection System at 1400 mA, 20 ms, 1 pulse. After 48 h, cells were stimulated with poly(I:C) and were subjected to RT-qPCR and WB analysis.

Table 2.4 Sequence of siRNA

Name	Sequence (5'-3')
siRNA_Nup93(sense)	CTGAAGAATGAGAAAGATAATGCCTTG
siRNA_Nup93(anti-sense)	CAAGGCATTATCTTTCTCATTCTTCAG

2.12 IRF3 phosphorylation and nuclear translocation

2.12.1 IRF3 and NF-κB p65 phosphorylation

WT and Nup93 KO 1×10^6 cells/well were cultured into 6 wells plate and were stimulated with 1 µg/ml poly(I:C) for 1 h. and 3 h. using Lipofectamine 2000. Whole cell lysates (WCLs) were prepared and WB was performed by indicating antibodies at Table 2.3 (anti-IRF3, anti-phospho-IRF3).

2.12.2 Fluorescence microscopy

Coverslips were plated on 24 wells plate and were coated by poly-L-lysine for 30m (Sigma). Coverslips were washed by PBS 3 times. WT and Nup93 KO 1×10^5 cells/well in 24 wells plate were stimulated with poly(I:C) for 6 h. Cells were fixed with 4% paraformaldehyde (Nacalai) for 30 m and were washed three times with 0.02% TritonX-100 in PBS and permeabilized with PBS containing 100 mM glycine and 0.02% TritonX-100 for 30 m. Cells were incubated overnight with blocking solution 0.02% TritonX-100 1%BSA in PBS at 4 °C. Next, cells were incubated overnight with primary antibody in 0.02% TritonX-100 1%BSA in PBS at 4 °C. Cells were washed three times and were incubated for 2 h with secondary antibody conjugated to Alexa 488. Nuclei were stained with Hoechst 33342. Coverslips were mounted with Fluoro-KEEPER Anti-fade Reagent (Nacalai Tesque). Fluorescence images were obtained by LSM700 (Carl Zeiss) and cell counts were performed with ImageJ.

2.13 Preparing deletion mutant plasmid

Nup93 deletion (Nup93Δ) amplification was divided to 3 steps: first, Nup93Δ was amplified from list of primers Table 2.2 (Nup93_EcoRI_F and Nup93_del1_R, Nup93_del2_F and Nup93_BamHI_R). Next, first PCR products were mixed and annealed without Nup93_EcoRI_F/Nup93_BamHI_R primers for second step PCR under the condition 94°C 2 m, 15 cycles of 94°C 30 s 60°C 2 m 68° C 5 m, 68°C 10 m and 4° C. The third step PCR was amplified from second step PCR using Nup93_EcoRI_F and Nup93_BamHI_R primers. The final PCR products were cloned into pFlag-CMV2 expression vector same as describe above.

2.14 Luciferase reporter assay

2.14.1 Reporter plasmid

IFN-β promoter activity was measured by Dual-Luciferase Reporter assay (Promega). pGL3-IFN-β-Luc plasmid containing a firefly luciferase gene downstream of IFN-β promoter, was used as a reporter plasmids and pTK-Luc plasmid containing Renilla luciferase gene downstream of the TK promoter was used as an internal control.

2.14.2 HEK 293 cells preparation and transfection

HEK293T cells were cultured in 24 wells plates with cell density of 50-70% or number of cells 1×10^5 cells/well 37°C 5% CO_2 incubator. Then, 50 ng/well of pGL3-IFN-β-Luc, 10 ng pTK-Luc, 250 ng of pFLAG-CMV Nup93, pFLAG-CMV Nup93Δ and pGST-TBK1 expression plasmids were mixed by using Opti-MEM (Life Technologies) and was adjusted to 50 μl. Plasmids were mixed with 50 μl of Opti-MEM containing polyethyleneimine (Polysciences, Inc.) and mixed solutions were incubated for 15 m. Then, mixed solutions were applied to the HEK293T cells culture supernatant. After 6 h, medium was replaced and carried out overnight.

2.14.3 Luciferase reporter assay

After 24 or 48 hours post transfection, the medium was removed and added 100 μl of 5× Passive Lysis Buffer (Promega) for dissolving the cells. Cell lysates were dispensed at 10 μl in 96 well plates. Firefly and Renilla luciferase activities were detected by TriStar[2] LB942 Multidetection Microplate Reader (Berthold) with Luciferase Assay Reagent II Stop & Glo Reagent (Promega). Promoter activities of the IFN-β from Firefly were normalized by Renilla

luciferase as an internal control promoter activity. Promoter activity = Firefly luciferase activity / Renilla luciferase activity

2.15 Co-immunoprecipitation and Immunoprecipitation

HEK293T 1×10^7 cells/well were cultured in 10 cm dish for overnight and were transfected with GST-TBK1, FLAG-Nup93 and control expression plasmids. After 24-48h, Cells were collected and were lysed by lysis buffer. Lysates were sonicated by 0.2 μm 20 % amplitude sonication and were centrifuged for 15 m at 13,500 rpm. Supernatants were transferred to new centrifuge tubes and were incubated with anti-FLAG antibody agarose beads (Sigma) and were rotated for 3 h at 4°C. Beads were collected by centrifuge 5,000 rpm 5 m 4°C and were washed for 3 times with lysis buffer. Sample buffer was applied to beads and samples were subjected to WB against anti-GST and anti-FLAG antibodies. GST-pull down experiment was performed with Glutathione (GST)-sepharose beads (GE healthcare).

3. Results

3.1 Expression of Nup93 in mouse BMMs

To determine the transcription of Nup93 during innate immune activation, BMMs were stimulated with LPS (TLR4 agonist) for 2 h, poly(I:C) (RIG-I agonist) for 6 h and ISD (cGAS agonist) for 6 h. Then, *Nup93* expression was measured by RT-qPCR. I found that the *Nup93* transcription levels were significantly upregulated by these stimulation (Figure 3.1). These results suggested that Nup93 is an inducible gene and may be involved in innate immune regulation.
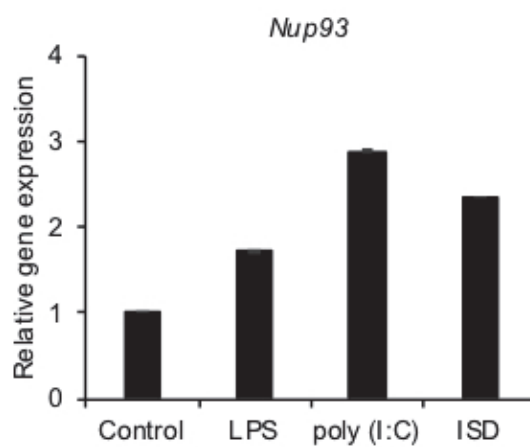
Figure 3.1 Expression of *Nup93* in BMMs. BMMs were stimulated with LPS, poly (I:C) and ISD and expression of *Nup93* gene was quantified by RT-qPCR. *Gapdh* was used as an internal control.

3.2 Generation of Nup93 knockout RAW264.7 cells

To investigate the functional role of Nup93 in innate immune signaling, I generated Nup93-deficient cells by CRISPR/Cas9 genome editing system. Murine macrophage like cell line, RAW264.7 cells were co-transfected with gRNA expression plasmid which targets to exon 4 in Nup93 together with CRISPR/Cas9 expression plasmid. Cells having insertion or deletion were selected by genome sequencing analysis (Figure 3.2A). Then, expression of Nup93 was confirmed by WB with anti-Nup93 antibody. I obtained cells with insertion of 14 and deletion of 11 base in exon4 sequence and used it as Nup93 Knockout (KO) cells (Figure 3.2B).
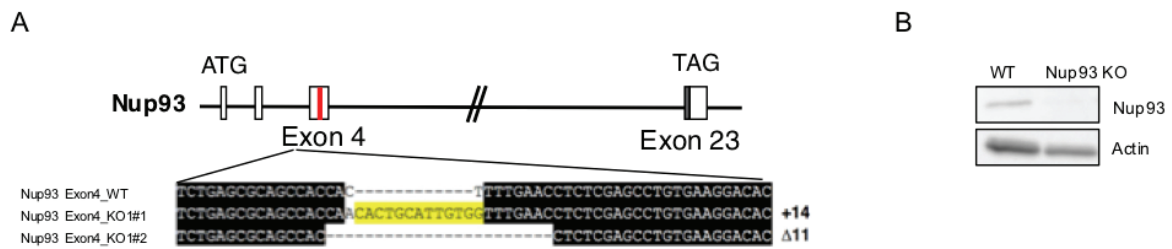
Figure 3.2 Generation of Nup93 KO RAW264.7 Cells (A) A schematic drawing of the Nup93 gene. Nup93 exon map and the mutation site are depicted. Partial sequences of the exon 4 are shown. (B) Cell lysates from WT and Nup93 KO cells were subjected to WB with anti-Nup93 and anti-Actin antibodies.

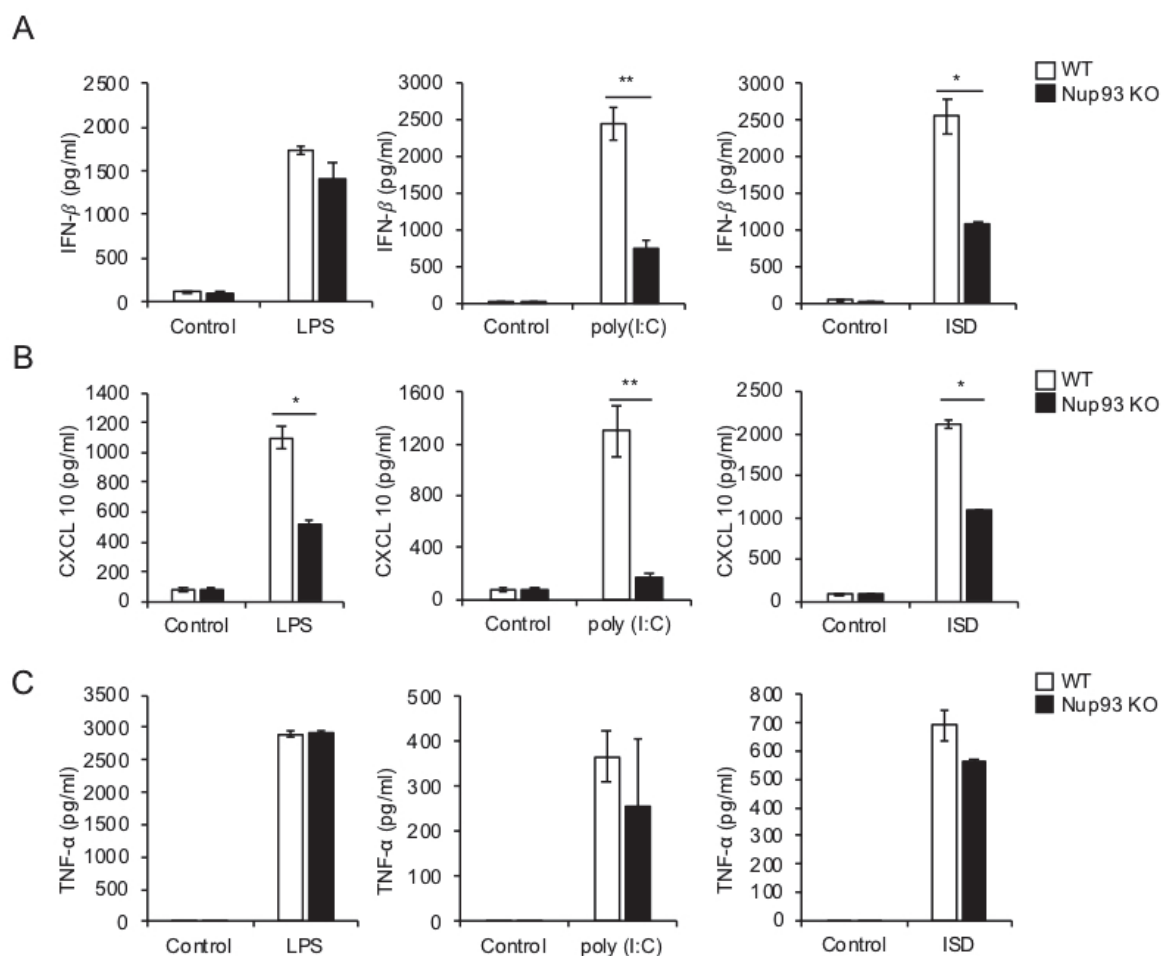## 3.3 Nup93-deficiency reduced *Ifnb1*, *Il6* and *Cxcl10* mRNA expression by LPS, poly(I:C) and ISD stimulation

WT and Nup93 KO RAW264.7 cells were stimulated with LPS, poly(I:C) and ISD. Expression of cytokine genes such as *Ifnb1*, *Il6, Cxcl10* and *Tnfa* were measured by RT-qPCR. Expression of *Ifnb1*, *Il6* and *Cxcl10* was significantly reduced in Nup93 KO cells compared with WT cells (Figure 3.3A-C) whereas expression of *Tnfa* was comparable between Nup93 KO and WT cells (Figure 3.3D). *Ifnb1*, *Il6* and *Cxcl10* mRNA induction is shown to be mainly regulated by IRF3 and NF-κB while *Tnfa* mRNA induction solely depends on NF-κB. These results therefore suggest that Nup93 regulates expression of IRF-dependent genes rather than NF-κB-dependent after LPS, poly(I:C) and ISD stimulation.
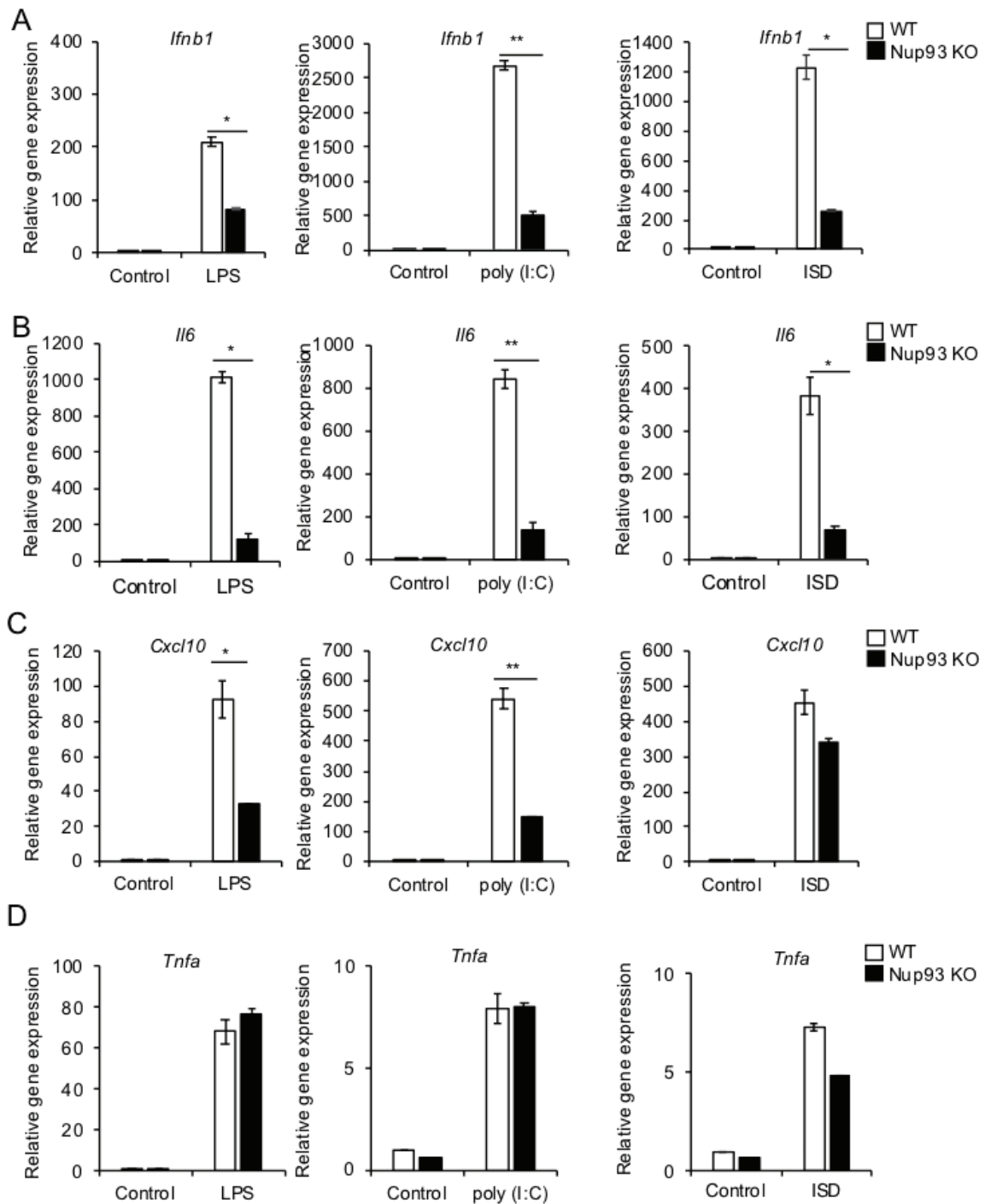
Figure 3.3 Nup93 deficiency reduced *Ifnb1*, *Il6* and *Cxcl10* expression after LPS, poly(I:C) and ISD stimulation. (A-D) WT and Nup93 KO RAW264.7 cells were stimulated with LPS, poly(I:C) or ISD and expression of (A) *Ifnb1,* (B) *Il6,* (C) *Cxcl10* and (D) *Tnfa* was measured by RT-qPCR. *Gapdh* was used as an internal control. Data are representative of three independent experiments, and mean values and SEs are depicted. ∗p < 0.05, ∗∗p < 0.01 paired Student's t test.

3.4 Nup93-deficency reduced IFN-β and CXCL10 production

To confirm further, IFN-β, TNF-α and CXCL10 in the culture supernatant was measured after stimulation with LPS, poly(I:C) and ISD. Production of IFN-β and CXCL10 was significantly reduced in Nup93 KO cells (Figure 3.4A, B), excepting for IFN-β production after LPS stimulation (Figure 3.4A). However, the production of TNF-α after LPS, poly (I:C) and ISD in Nup93 KO cells was comparable with that in WT cells (Figure 3.4C).

Figure 3.4 Nup93 deficiency reduced production of IFN-β and CXCL10 after LPS, poly(I:C) and ISD stimulation. WT and Nup93 KO RAW264.7 cells were stimulated with LPS, poly(I:C) or ISD. Productions of (A) IFN-β (B) CXCL10 and (C) TNF-α in the supernatant were measured by ELISA assay. N = 3; mean values and SEs are depicted. ∗p < 0.05 paired Student's t test ∗∗p < 0.01 paired Student's t test.

3.5 Nup93-deficiency reduced *Ifnb1*, *Il6* and *Cxcl10* mRNA expression during NDV virus infection

To investigate physiological role of Nup93 during viral infection, WT and Nup93 KO cells were infected with NDV which is sensed by RIG-I and expression of *Ifnb1*, *Il6*, *Cxcl10* and *Tnfa* was measured by RT-qPCR. *Ifnb1*, *Il6* and *Cxcl10* mRNA expression was significantly reduced compared with WT after NDV infection (Figure 3.5 A). However, *Tnfa* mRNA expression after NDV infection was not significantly reduced in Nup93 KO cells.
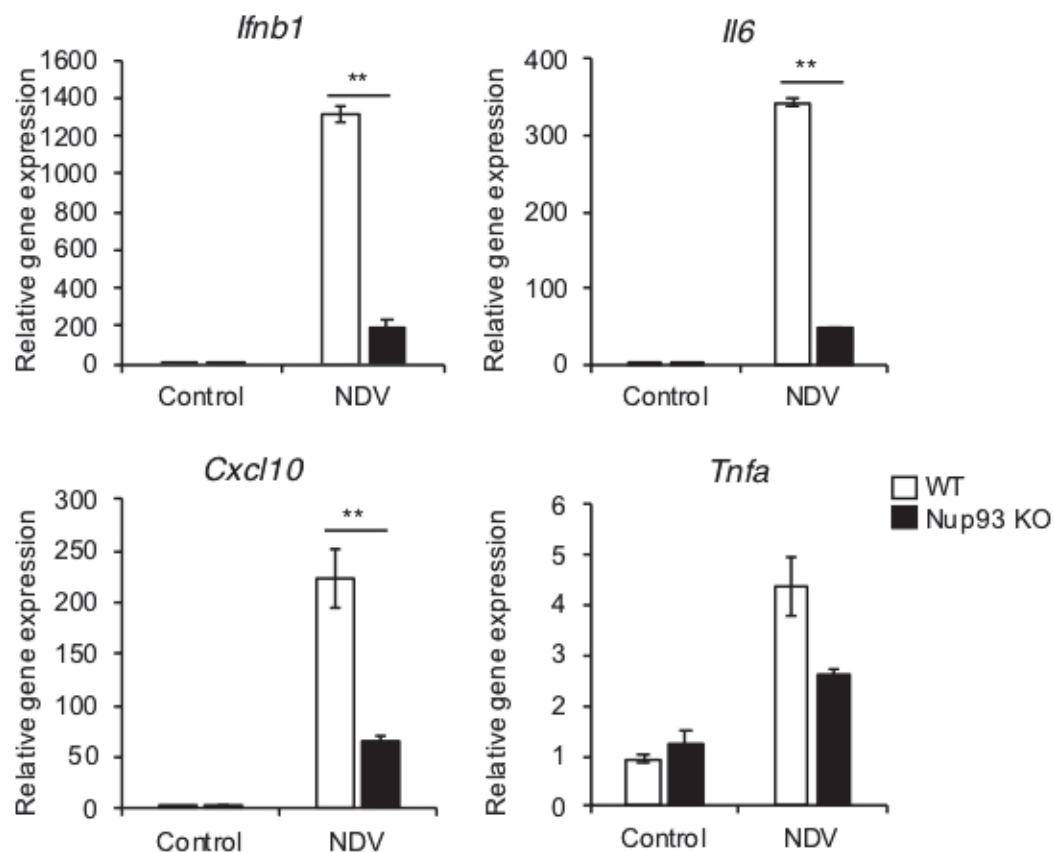
Figure 3.5 Nup93-deficiency reduced *Ifnb1*, *Il6*, *Cxcl10* mRNA expression during NDV virus infection

WT and Nup93 KO RAW264.7 cells were infected with NDV at MOI = 10 and *Ifnb1*, *Il6*, *Cxcl10* and *Tnfa* mRNA expression was measured after NDV infection. *Gapdh* was used as an internal control. N = 3; mean values and SEs are depicted. *$p < 0.05$ paired Student's t test **$p < 0.01$ paired Student's t test.

### 3.6 Nup93-deficiency restored by exogenously Nup93

To restore Nup93 expression into Nup93 KO cells, Nup93 KO cells were infected with retrovirus expressing FLAG-tagged Nup93. Expression of FLAG-Nup93 in Nup93 KO cells was confirmed by WB analysis with anti-Nup93 and anti-FLAG antibodies (Figure 3.6A). Exogenous expression of FLAG-Nup93 in Nup93 KO cells restored *Ifnb1* mRNA expression in response to poly(I:C) stimulation as measured by RT-qPCR (Figure 3.6B).
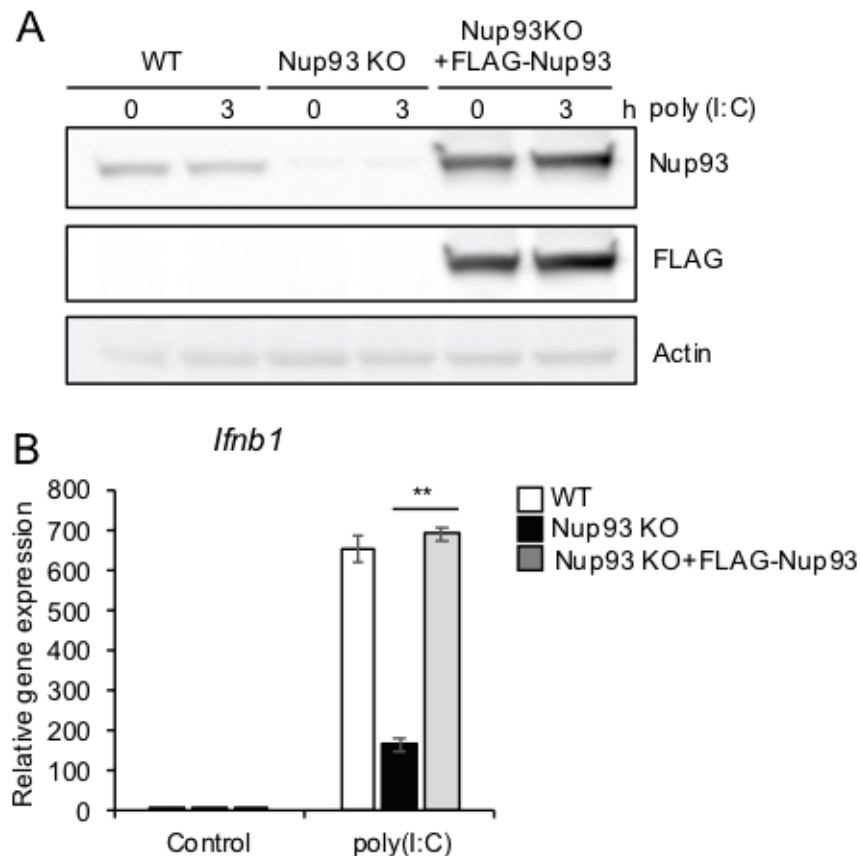
Figure 3.6 Expression of FLAG-Nup93 into Nup93 KO cells recovered *Ifnb1* mRNA expression after poly(I:C) stimulation. (A) Nup93 KO cells were infected with retroviruses encoding FLAG-Nup93. Nup93 expression was confirmed by WB using the indicated antibodies. (B) WT, Nup93 KO and Nup93 KO + FLAG-Nup93 cells were stimulated with poly(I:C) and *Ifnb1* mRNA expression was measured by RT-qPCR. *Gapdh* used as an internal control. Data are representative of three independent experiments, and mean values and SEs are depicted. $*p < 0.05$, $**p < 0.01$ paired Student's t test.

3.7 Nup93 knockdown inhibited IFN-β induction

To investigate functional roles of Nup93 in primary cells. Nup93 was knocked down in BMMs and MEFs. BMMs and MEFs were electroporated with siRNA for control and Nup93 and expression of Nup93 was confirmed by WB (Figure 3.7 A, D) and RT-qPCR (Figure 3.7 B, E). Then, siRNA treated cells were stimulated with poly(I:C) and *Ifnb1*, *Cxcl10* and *Il6* expression was measured by RT-qPCR. Expression of these cytokines was decreased by Nup93 knockdown (Figure 3.7 C, F).
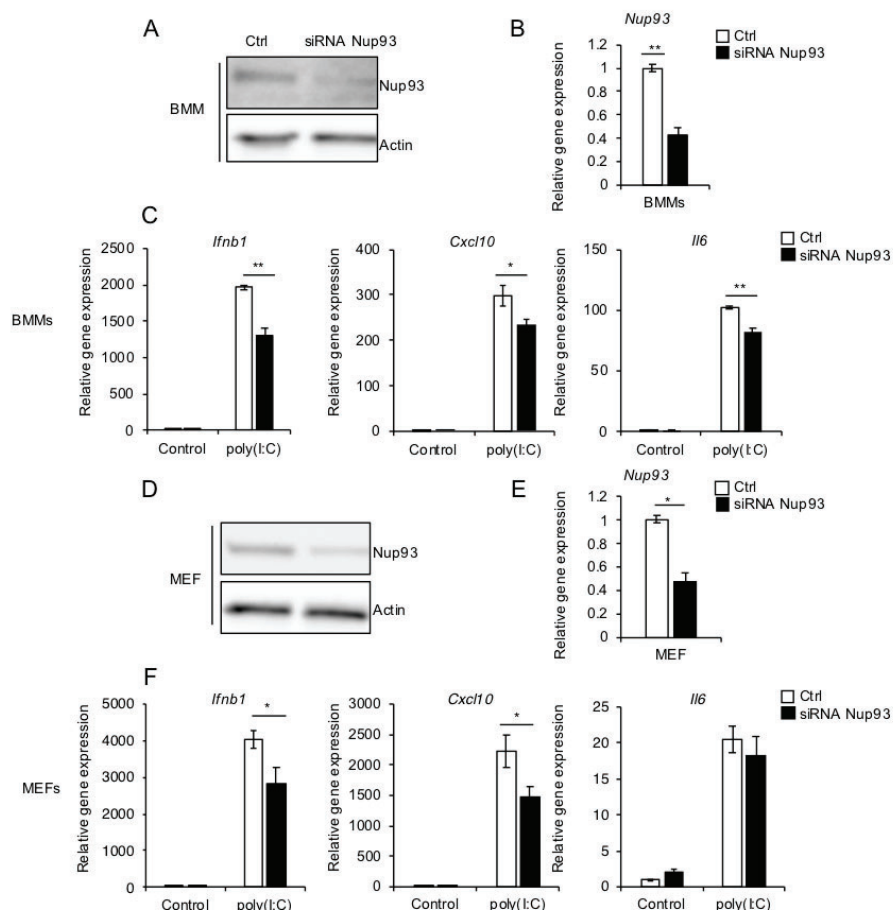
Figure 3.7 Nup93 knockdown inhibited IFN-β induction after poly(I:C) stimulation. (A, B) BMMs were electroporated with siRNA for control or Nup93, and expression of Nup93 was examined by WB (A) and RT-qPCR (B). (C) *Ifnb1*, *Cxcl10* and *Il6* mRNA expression in BMMs after poly(I:C) stimulation was measured by RT-qPCR. (D, E) MEFs were electroporated with siRNA and expression of Nup93 was confirmed by WB (D) and RT-qPCR I. (F) *Ifnb1*, *Cxcl10* and *Il6* mRNA expression in MEFs after poly(I:C) stimulation was measured by RT-qPCR. *Gapdh* used as an internal control. Data are representative of three independent experiments, and mean values and SEs are depicted. $*p < 0.05$, $**p < 0.01$ paired Student's t test.

3.8 Nup93 was required for IRF3 nuclear translocation following RLR induction

To examine the role of Nup93 in RLR signaling pathway, IRF3 phosphorylation and nuclear translocation was examined. WT and Nup93 KO cells were stimulated with poly(I:C) and WCLs were subjected to WB against anti-IRF3 and anti-phosphorylated IRF3 antibodies (Figure3.8A). IRF3 phosphorylation was significantly reduced in Nup93 KO cells compared with WT. Then, cells were stained with anti-IRF3 antibody for visualization of IRF3 cellular localization. IRF3 translocated from cytosol to nucleus after poly(I:C) stimulation in WT cells, with around 60% of cells, whereas around 30% of Nup93 KO cells showed IRF3 nuclear translocation (Figure 3.8B). These results suggest that Nup93 was required for IRF3 phosphorylation and nuclear translocation following RLR induction.
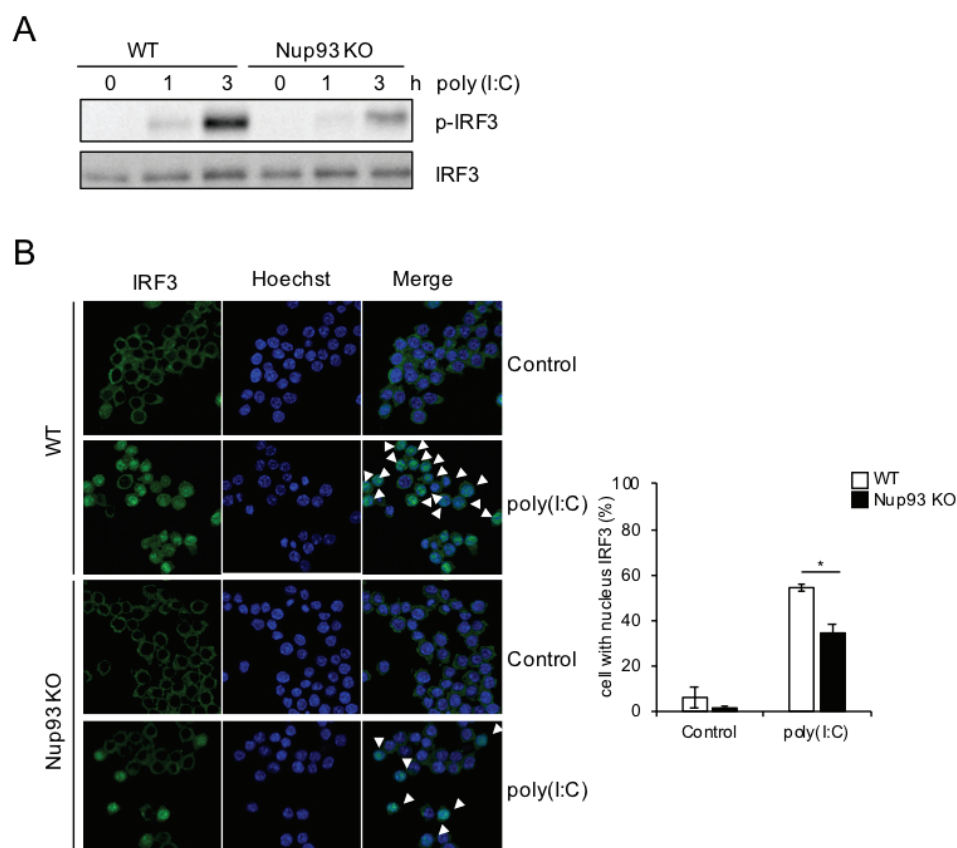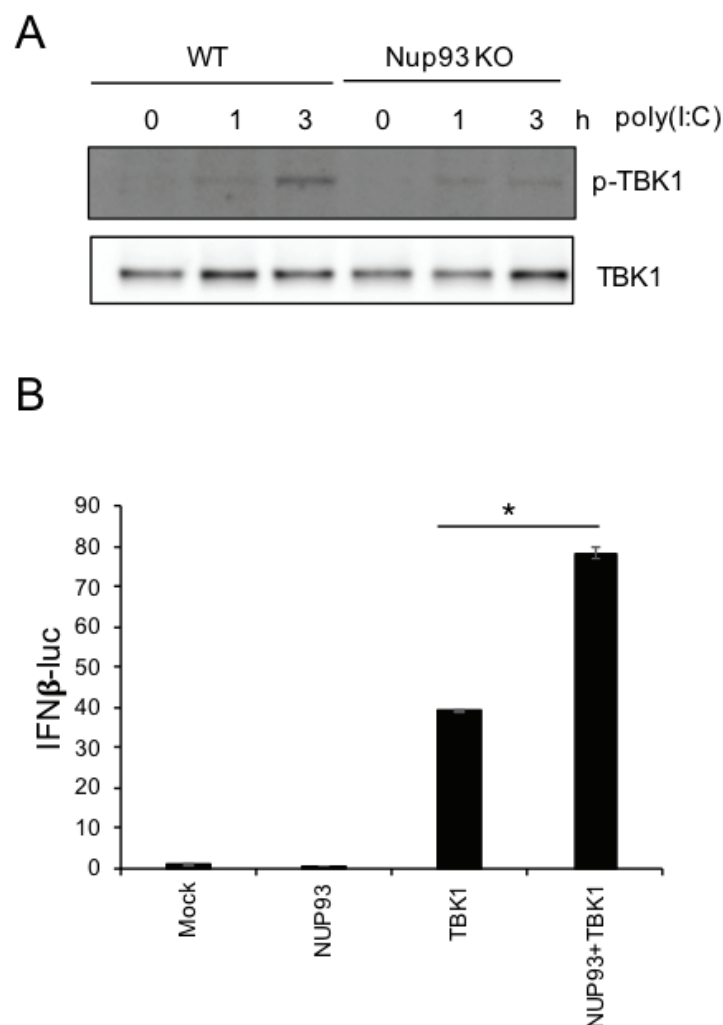

Figure 3.8 Nup93 was required for IRF3 nuclear translocation following RLR induction. (A) WT and Nup93 KO cells were stimulated with poly(I:C). WCLs were immunoblotted with the indicated antibodies. (B) WT and Nup93 KO cells stimulated with or without poly(I:C) were stained with anti-IRF3 antibody (green) and Hoechst 33342 (blue). Cell images were collected with confocal microscope (Left). Cells with nuclear IRF3 were counted and bar graph showed the percentage of nuclear located cells in total cells (right). N = 3; mean values and SEs are depicted. *p < 0.05 paired Student's t test.

### 3.9 Phosphorylation of TBK1 was reduced in Nup93 KO cells following RLR induction

To determine whether Nup93 is involved in TBK1 activation, WT and Nup93 KO cells were stimulated with poly(I:C) and WCLs from them were subjected to WB witht anti-phosphorylated-TBK1 antibody. TBK1 phosphorylation after poly(I:C) stimulation was decreased in Nup93 KO cells in comparison with WT cells (Figure 3.10A). In addition, IFN-β promoter activity induced by TBK1 overexpression was increased by co-overexpression with Nup93. These results suggest that Nup93 regulates RLR signaling by controlling TBK1 activation (Figure 3.10B).

Figure 3.9 TBK1 activation was reduced in Nup93 KO cells following RLR induction (A) WT and Nup93 KO cells were stimulated with poly(I:C) (A) WCLs were immunoblotted with the indicated antibodies. (B) HEK293T cells were transfected with TBK1 expression plasmid along with or without Nup93 and the luciferase activity was measured. N = 3; mean values and SEs are depicted. *p < 0.05 paired Student's t test.

3.10 Nup93 mutant failed to enhance IFN-β promoter activity induced by TBK1

To understand regulatory role of Nup93 in RLR-mediated innate immune response, I constructed a deletion mutant of Nup93 at β sheet in NIC96 domain (Nup93Δ) (Figure 3.11A). Nup93Δ has a deletion of glycine (G), serine (S), arginine (R) in 591-594 amino acids. Then, Nup93Δ was co-transfected with TBK1 along with the luciferase reporter plasmid driven by IFN-β promoter in HEK293T cells. IFN-β promoter activity induced by TBK1 overexpression was further enhanced by co-expression with Nup93, however it was not enhanced by co-expression with Nup93Δ. These results suggest that β sheet at NIC96 domain in Nup93 required for TBK1 activation (Figure 3.11B).
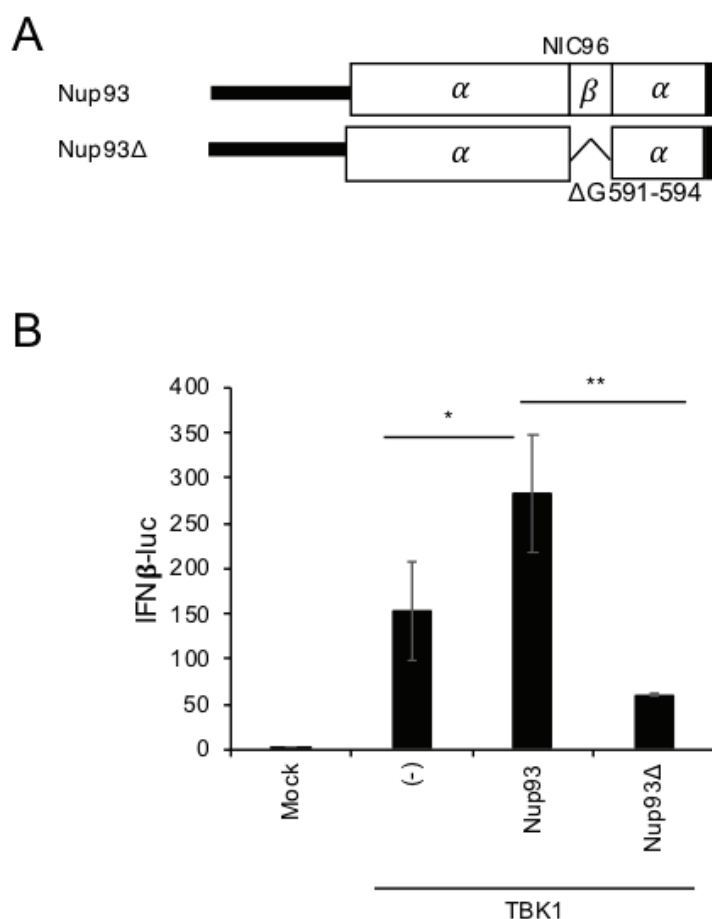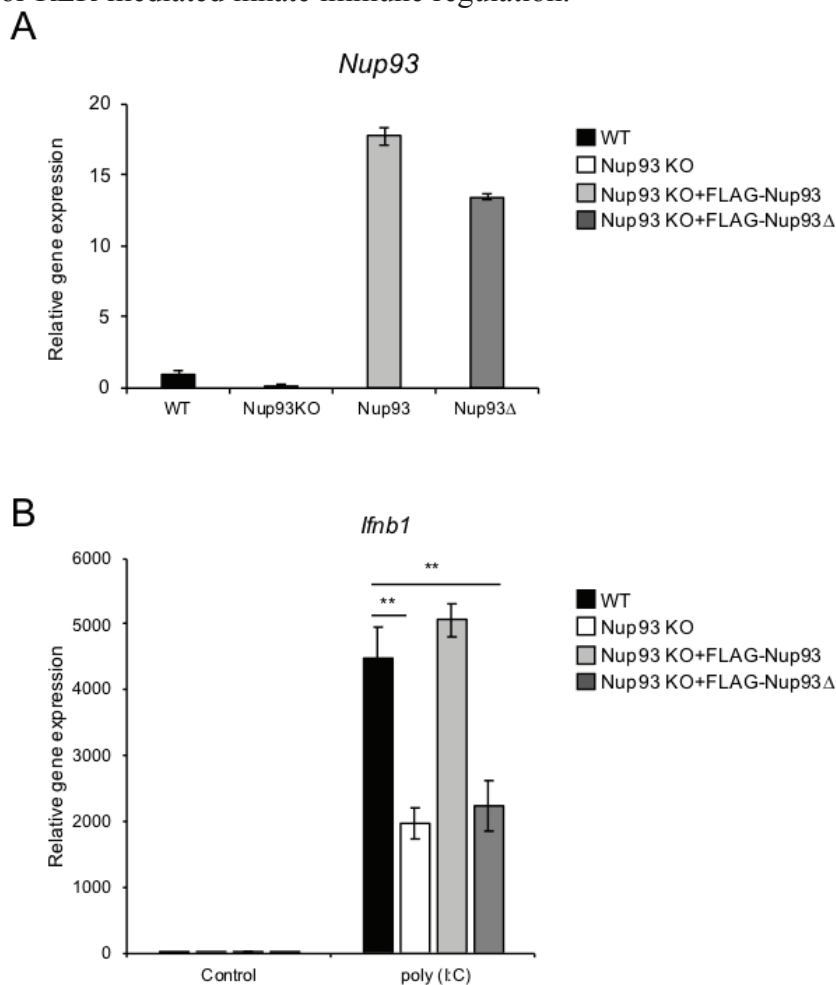

Figure 3.10 Nup93 mutant reduced production of IFN-β by RLR ligands

(A) Schematic diagrams of Nup93 and Nup93 deletion mutant. (B) HEK293T cells were co-transfected with Mock, FLAG-Nup93, FLAG-Nup93Δ and TBK1 along with luciferase reporter plasmid driven by IFN-β promoter. Luciferase activity was measured after 24 h post transfection. Data are representative of three independent experiments, and mean values and SEs are depicted. $*p < 0.05$, $**p < 0.01$ paired Student's t test.

3.11 Nup93 mutant reduced expression of IFN-β after poly(I:C) stimulation

Nup93Δ was transfected into Nup93 KO cells and *Ifnb1* expression was measured after poly(I:C) stimulation. Expression of Nup93WT and Nup93Δ was measured by RT-qPCR and those were highly expressed, comparing with endogenous level (Figure 3.12A). WT Nup93 restored expression of *Ifnb1* after poly(I:C) stimulation, however Nup93Δ failed to restore the expression (Figure 3.12B). These results suggest that β sheet site at NIC96 domain of Nup93 is required for RLR-mediated innate immune regulation.

Figure 3.11 FLAG-Nup93 mutant in Nup93 KO cells reduced production of IFN-β by RLR ligands

(A) Nup93 KO cells were infected with retrovirus encoding FLAG-Nup93 or FLAG-Nup93Δ. Expression of WT and mutant Nup93 was measured by RT-qPCR. (B) WT, Nup93 KO and Nup93 KO + FLAG-Nup93 or FLAG-Nup93Δ cells were stimulated with poly(I:C) and *Ifnb1* expression was measured by RT-qPCR. *Gapdh* was used as an internal control. Data are representative of three independent experiments, and mean values and SEs are depicted. $*p < 0.05$, $**p < 0.01$ paired Student's t test.
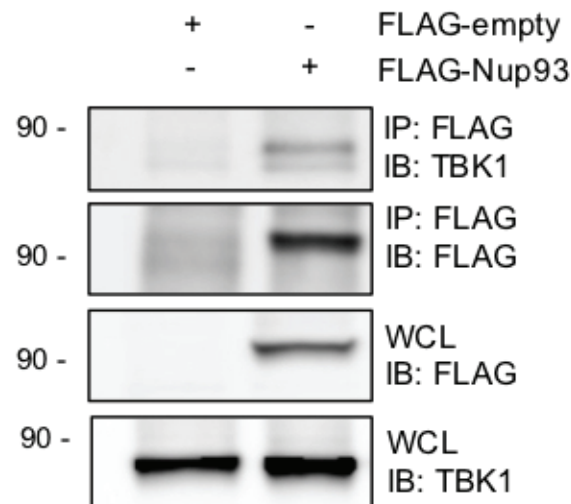
3.12 Nup93 interacted with TBK1

To examine the interaction between Nup93 with TBK1, FLAG-Nup93 was co-transfected with GST-tagged TBK1 into HEK293T cells, and co-immunoprecipitation was conducted. FLAG-Nup93 was co-precipitated with Glutathione (GST) sepharose beads from lysates prepared from cells expressing FLAG-Nup93 and GST-TBK1 (Figure 3.1A). Furthermore, GST-TBK1 was co-immunoprecipitated with anti-FLAG antibody from cell lysates containing FLAG-Nup93 (Figure 3.13B). Thus, these results suggest that GST-TBK1 and FLAG-TBK1 form a complex.
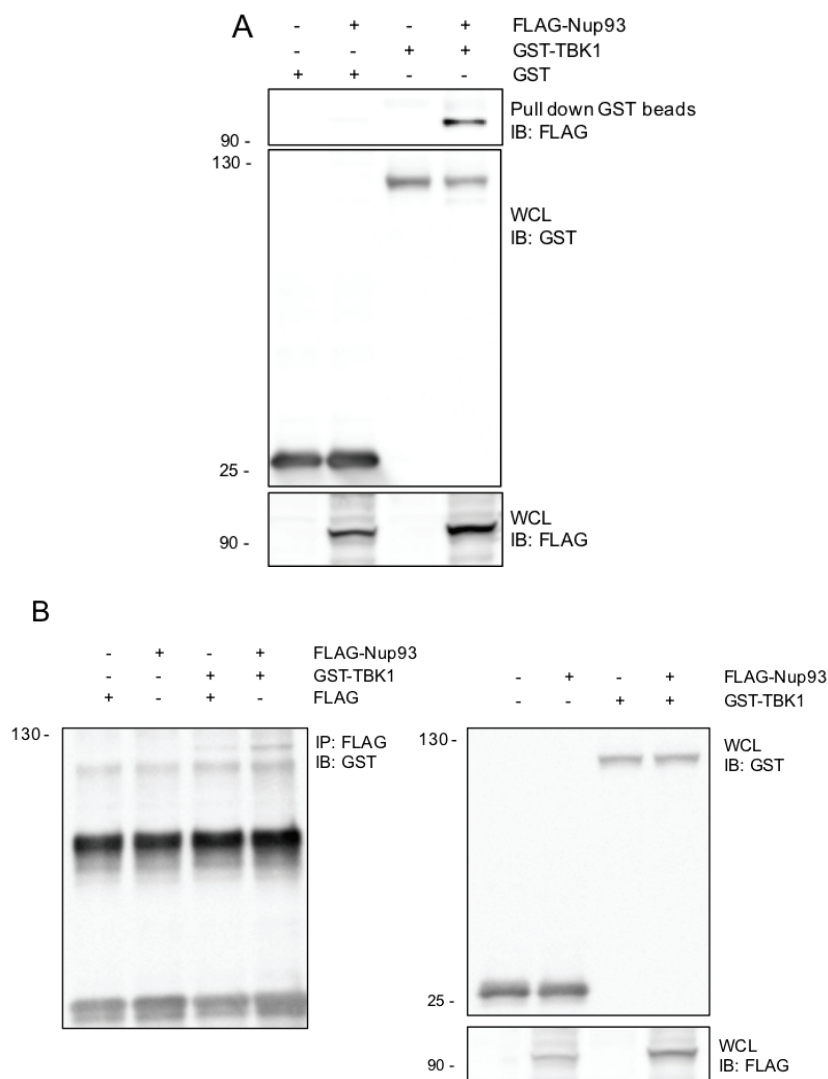
Figure 3.12 Nup93 interacted with TBK1 (A, B) HEK293T cells were transfected with FLAG, GST, FLAG-Nup93 and GST-TBK1 expression plasmids as indicated. (A) GST proteins were pulled down by Glutathione sepharose beads (B) FLAG-tagged proteins were precipitated by IP with anti-FLAG antibody sepharose. WCLs and beads bounded proteins were separated by SDS-PAGE and WB were detected by indicated antibodies (A, B).

3.13 Overexpressed Nup93 interacted with endogenous TBK1

I further analyzed whether endogenous TBK1 associates with FLAG-Nup93. In this regard, I overexpressed FLAG-Nup93 into RAW264.7 cells and WCLs were precipitated with anti-FLAG antibody and blotted with anti-TBK1 antibody. The endogenous TBK1 was co-precipitated with FLAG-Nup93, suggesting that endogenous TBK1 associates with FLAG-Nup93 (Figure 3.14).
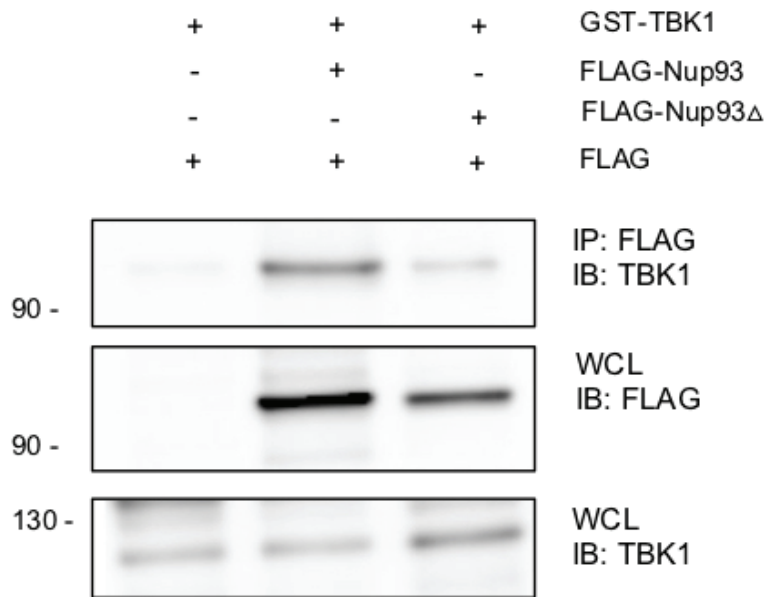

Figure 3.13 Overexpressed Nup93 interacted with endogenous TBK1

FLAG-empty of FLAG-Nup93 was overexpressed in RAW264.7 cells. WCLs were precipitated with anti-FLAG antibody and precipitant were subjected to WB against anti-TBK1 or anti-FLAG antibody. WCLs were simultaneously blotted with anti-TBK1 or anti-FLAG antibody.

3.14 Nup93 deletion mutant lowered the interaction with TBK1

To examine whether Nup93Δ interacts with TBK1, FLAG-Nup93 WT or FLAG-Nup93Δ was co-expressed with GST-TBK1 in HEK293T cells and WCLs were precipitated with anti-FLAG antibody. Nup93 was associated with TBK1, but association of Nup93Δ with TBK1 was weaker than that of Nup93 WT (Figure 3.15). These results suggest that NIC96 domain in Nup93 is required for a robust interaction with TBK1.

Figure 3.14 Nup93 deletion mutant lowered the interaction with TBK1

GST-TBK1 was co-expressed with FLAG-Nup93 or FLAG-Nup93Δ in HEK293T cells. WCLs were precipitated with anti-FLAG antibody and were blotted with anti-FLAG or anti-TBK1 antibody. WCLs were simultaneously blotted with anti-TBK1 antibody.

4. Discussion

In this study, I have focused on Nups which are evolutionally conserved in distant eukaryotes ranging from yeast to human, and identified Nup93, a subunit of nuclear pore complex, as a regulator in antiviral innate immunity. Nup93 gene was upregulated after LPS, poly(I:C) and ISD stimulation (Figure 3.1A), suggesting that Nup93 is an inducible gene upon infection that modulates innate immune responses. Nup93 deficiency impaired *Ifnb1*, *Il6* and *Cxcl10* expression and production of IFNβ and CXCL10 after those stimulations, excepting IFNβ production by LPS stimulation (Figure 3.3, 3.4). Moreover, Nup93 deficiency also suppressed *Ifnb1* expression after NDV infection (Figure 3.5). Notably, IRF3 phosphorylation and nuclear translocation were impaired by Nup93 deficiency. Accordingly, expression of IRF3 dependent gene; *Ifnb1*, *Il6* and *Cxcl10* was impaired by Nup93 deficiency whereas expression of NF-κB dependent gene; *Tnfa* was not altered. Thus, these results suggest that Nup93 positively mediates RLR-IRF3-dependent antiviral innate immune responses.

Nups form NPC, and Nup family gene deficiency is expected to disrupt nuclear pore formation and dysregulate target protein transport between nucleus and cytoplasm. It was shown that depletion of Nup93 in *Xenopus laevis* reduced nuclear assembly (Grandi et al., 1997; Sachdev et al., 2012). Nup93 was also shown to be important for a recruitment of Nup62 complex, which establishes the permeability barrier and transport competency of NPC (Sachdev et al., 2012). Indeed, Nup93 knockdown suppresses nuclear transport of SMAD4 during bone morphogenetic protein-7 (BMP7) stimulation (Braun et al., 2016). Thus, it is considered that Nup93 deficiency impairs IRF3 translocation from cytosol to nucleus. However, I found that IRF3 phosphorylation, which occurs prior to nuclear translocation, was reduced in Nup93 KO cells (Figure 3.8A). Therefore, Nup93 might regulate IRF3 nuclear translocation as well as phosphorylation. Upon virus infection, TBK1 is auto-phosphorylated to become an active form to catalyze IRF3 phosphorylation in the cytoplasm. Phosphorylated IRF3 is dimerized and translocated to nuclei where it induces the transcription of type I IFN and other target genes (Kawai and Akira, 2006). I found that phosphorylated-TBK1 appeared to be reduced in Nup93 KO cells (Figure 3.9). Moreover, the IFNβ promoter activity induced by TBK1 overexpression was further increased in the presence of Nup93. These results suggest that Nup93 regulates TBK1 activation. Nup93 contained NIC96 domain which is important for interaction with other Nup family proteins and transport regulatory proteins. Mutation of Glycine 591 in NIC96 domain on Nup93 abrogated the interaction with Importin 7 (Braun et

al., 2016). From this notion, I generated deletion mutant that targets β sheet between α helix in NIC96 domain which contained Glycine 591. Importantly, Nup93 mutant failed to enhance the promoter activity induced by TBK1 overexpression and Nup93Δ failed to rescue *Ifnb1* expression in Nup93 KO cells (Figure 3.9, 3.11). These findings collectively suggest that Nup93 regulates TBK1 activation via the NIC96 domain.

Nups are known as the nuclear pore complex that regulates functions of nucleocytoplasmic transport (Beck and Hurt, 2017; Ibarra and Hetzer, 2015; Knockenhauer and Schwartz, 2016); however, recent studies suggested that Nups are synthesized as soluble proteins in cytoplasm. Nups have mobility both on and off with nuclear membrane (Cronshaw et al., 2002; Rabut et al., 2004). Indeed, part of Nups including Nup88, Nup214, Nup205 in human cells showed localization at cytoplasmic puncta known as stress granule (Zhang et al., 2018). I also observed localization of Nup93 in cytosol (data not shown). Therefore, Nup93 may have a bifunctional role which regulates TBK1 activity as well as NPC formation. Furthermore, I found that Nup93 interacts with TBK1 and its interaction was reduced by deletion of β sheet at NIC96 domain in Nup93 although TBK1 and Nup93 interaction was still detectable, suggesting that β sheet at NIC96 domain in Nup93 is required for TBK1 interaction which maximizes its activities, but the other region in Nup93 is also required for association with TBK1. A previous report from Wang and colleagues showed that the ubiquitin chains create an anchoring platform for recruiting and activating TBK1 to the perinuclear microsomes (Wang et al., 2014). It may be possible that Nup93 interacts with TBK1 when TBK1 is recruited to the nuclear membrane along with perinuclear microsomes, which should be investigated in the future.

Here I found that Nup93 enhances activation of TBK1. Nup93 may also regulate transport of phosphorylated IRF3 from cytosol to nucleus. Nup93 may bifunctionally work for the regulation of activation of cytosolic signaling molecule as well as nuclear transport via NPC formation. However, additional studies are needed to elucidate the mechanism underlying innate immune regulation by Nup93. As described in the introduction, Nup93 is a conserved gene among several species. Innate immune response is also one of well conserved host defense system. It is interesting to clarify innate immune regulation by Nup93 in other species as well.

Further work in examining the role of Nup93 in mammalian viral infection will lead to better understanding of the transcriptional regulation of immune system and may help us to develop potential therapeutic applications targeting viral diseases.
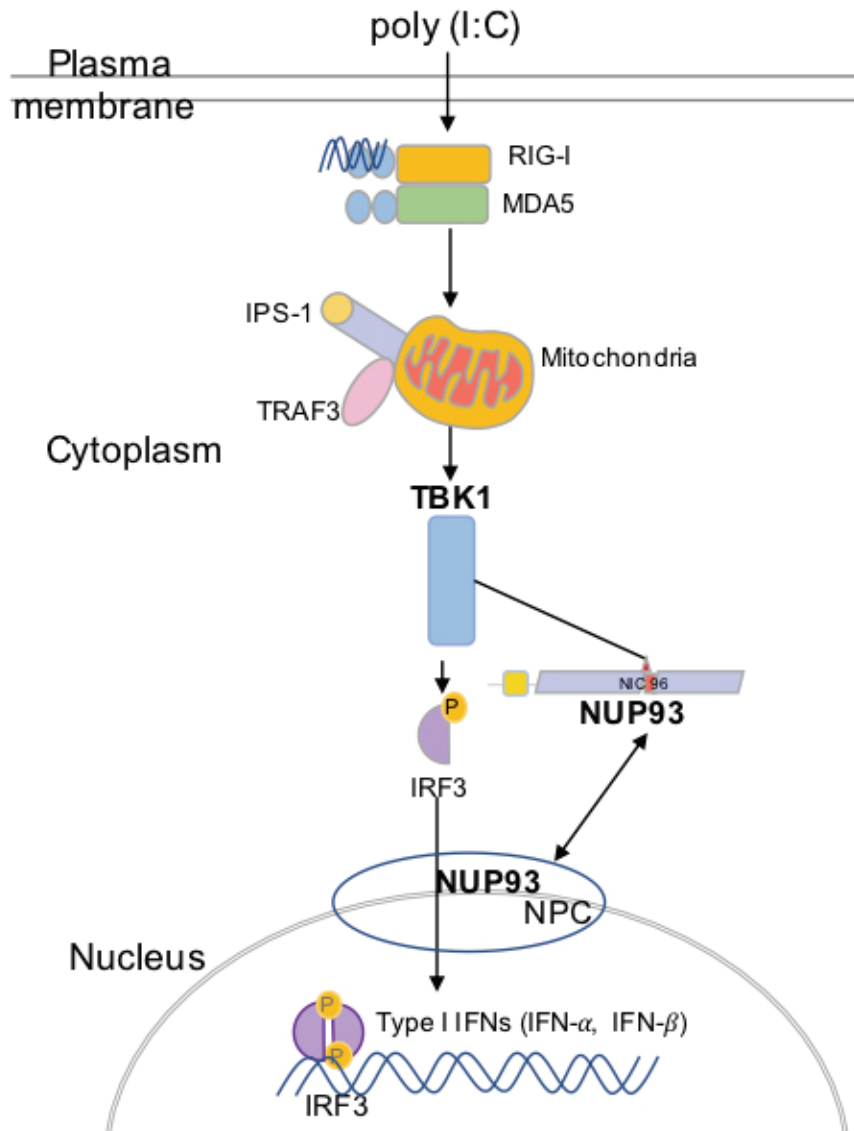
Figure 4.1 The predicted pathway of Nup93 following RLR induction. RLR pathway consists of RIG-I and MDA5, which bind to IPS-1. IPS-1 activates downstream signaling cascade leading to activation of TBK1 for type I IFNs expression, which interacts with Nup93 at NIC96 domain.

5. Acknowledgements

6. References

Ablasser, A., Goldeck, M., Cavlar, T., Deimling, T., Witte, G., Röhl, I., Hopfner, K.-P., Ludwig, J., and Hornung, V. (2013). cGAS produces a 2′-5′-linked cyclic dinucleotide second messenger that activates STING. Nature *498*, 380.

Akira, S., Uematsu, S., and Takeuchi, O. (2006). Pathogen recognition and innate immunity. Cell *124*, 783-801.

Baril, M., Es-Saad, S., Chatel-Chaix, L., Fink, K., Pham, T., Raymond, V.-A., Audette, K., Guenier, A.-S., Duchaine, J., and Servant, M. (2013). Genome-wide RNAi screen reveals a new role of a WNT/CTNNB1 signaling pathway as negative regulator of virus-induced innate immune responses. PLoS pathogens *9*, e1003416.

Barton, G.M. (2007). Viral recognition by Toll-like receptors. In Seminars in immunology (Elsevier), pp. 33-40.

Beck, M., and Hurt, E. (2017). The nuclear pore complex: understanding its function through structural insight. Nature reviews Molecular cell biology *18*, 73.

Braun, D.A., Sadowski, C.E., Kohl, S., Lovric, S., Astrinidis, S.A., Pabst, W.L., Gee, H.Y., Ashraf, S., Lawson, J.A., and Shril, S. (2016). Mutations in nuclear pore genes NUP93, NUP205 and XPO5 cause steroid-resistant nephrotic syndrome. Nature genetics *48*, 457.

Chen, M., Meng, Q., Qin, Y., Liang, P., Tan, P., He, L., Zhou, Y., Chen, Y., Huang, J., and Wang, R.-F. (2016). TRIM14 inhibits cGAS degradation mediated by selective autophagy receptor p62 to promote innate immune responses. Molecular cell *64*, 105-119.

Chug, H., Trakhanov, S., Hülsmann, B.B., Pleiner, T., and Görlich, D. (2015). Crystal structure of the metazoan Nup62• Nup58• Nup54 nucleoporin complex. Science *350*, 106-110.

Civril, F., Deimling, T., de Oliveira Mann, C.C., Ablasser, A., Moldt, M., Witte, G., Hornung, V., and Hopfner, K.-P. (2013). Structural mechanism of cytosolic DNA sensing by cGAS. Nature *498*, 332.

Cronshaw, J.M., Krutchinsky, A.N., Zhang, W., Chait, B.T., and Matunis, M.J. (2002). Proteomic analysis of the mammalian nuclear pore complex. The Journal of cell biology *158*, 915-927.

Dempsey, A., and Bowie, A.G. (2015). Innate immune recognition of DNA: A recent history. Virology *479*, 146-152.

Enninga, J., Levy, D.E., Blobel, G., and Fontoura, B.M. (2002). Role of nucleoporin induction in releasing an mRNA nuclear export block. Science *295*, 1523-1525.

Faria, A.M., Levay, A., Wang, Y., Kamphorst, A.O., Rosa, M.L., Nussenzveig, D.R., Balkan, W., Chook, Y.M., Levy, D.E., and Fontoura, B.M. (2006). The nucleoporin Nup96 is required for proper expression of interferon-regulated proteins and functions. Immunity *24*, 295-304.

Fredericksen, B.L., Keller, B.C., Fornek, J., Katze, M.G., and Gale, M. (2008). Establishment and maintenance of the innate antiviral response to West Nile Virus involves both RIG-I and MDA5 signaling through IPS-1. Journal of virology *82*, 609-616.

Gao, D., Wu, J., Wu, Y.-T., Du, F., Aroh, C., Yan, N., Sun, L., and Chen, Z.J. (2013). Cyclic GMP-AMP synthase is an innate immune sensor of HIV and other retroviruses. Science *341*, 903-906.

Gitlin, L., Barchet, W., Gilfillan, S., Cella, M., Beutler, B., Flavell, R.A., Diamond, M.S., and Colonna, M. (2006). Essential role of mda-5 in type I IFN responses to polyriboinosinic: polyribocytidylic acid and encephalomyocarditis picornavirus. Proceedings of the National Academy of Sciences *103*, 8459-8464.

Grandi, P., Dang, T., Pané, N., Shevchenko, A., Mann, M., Forbes, D., and Hurt, E. (1997). Nup93, a vertebrate homologue of yeast Nic96p, forms a complex with a novel 205-kDa protein and is required for correct nuclear pore assembly. Molecular biology of the cell *8*, 2017-2038.

Grossman, E., Medalia, O., and Zwerger, M. (2012). Functional architecture of the nuclear pore complex. Annual review of biophysics *41*, 557-584.

Hashimoto, T., Harita, Y., Takizawa, K., Urae, S., Ishizuka, K., Miura, K., Horita, S., Ogino, D., Tamiya, G., and Ishida, H. (2019). In vivo expression of NUP93 and its alteration by NUP93 mutations causing focal segmental glomerulosclerosis. Kidney International Reports.

Hoelz, A., Debler, E.W., and Blobel, G. (2011). The structure of the nuclear pore complex. Annual review of biochemistry *80*, 613-643.

Ibarra, A., and Hetzer, M.W. (2015). Nuclear pore proteins and the control of genome functions. Genes & development *29*, 337-349.

Ishikawa, H., and Barber, G.N. (2008). STING is an endoplasmic reticulum adaptor that facilitates innate immune signalling. Nature *455*, 674.

Kato, H., Takeuchi, O., Sato, S., Yoneyama, M., Yamamoto, M., Matsui, K., Uematsu, S., Jung, A., Kawai, T., and Ishii, K.J. (2006). Differential roles of MDA5 and RIG-I helicases in the recognition of RNA viruses. Nature *441*, 101.

Kawai, T., and Akira, S. (2006). Innate immune recognition of viral infection. Nature immunology *7*, 131-137.

Kawai, T., and Akira, S. (2010). The role of pattern-recognition receptors in innate immunity: update on Toll-like receptors. Nat Immunol *11*, 373-384.

Kawai, T., Takahashi, K., Sato, S., Coban, C., Kumar, H., Kato, H., Ishii, K.J., Takeuchi, O., and Akira, S. (2005). IPS-1, an adaptor triggering RIG-I-and Mda5-mediated type I interferon induction. Nature immunology *6*, 981.

Knockenhauer, K.E., and Schwartz, T.U. (2016). The nuclear pore complex as a flexible and dynamic gate. Cell *164*, 1162-1171.

Le Sage, V., and Mouland, A. (2013). Viral subversion of the nuclear pore complex. Viruses *5*, 2019-2042.

Li, C., Goryaynov, A., and Yang, W. (2016). The selective permeability barrier in the nuclear pore complex. Nucleus *7*, 430-446.

Li, T., and Chen, Z.J. (2018). The cGAS–cGAMP–STING pathway connects DNA damage to inflammation, senescence, and cancer. Journal of Experimental Medicine *215*, 1287-1299.

Li, X., Shu, C., Yi, G., Chaton, C.T., Shelton, C.L., Diao, J., Zuo, X., Kao, C.C., Herr, A.B., and Li, P. (2013). Cyclic GMP-AMP synthase is activated by double-stranded DNA-induced oligomerization. Immunity *39*, 1019-1031.

Liu, Y., Li, J., Chen, J., Li, Y., Wang, W., Du, X., Song, W., Zhang, W., Lin, L., and Yuan, Z. (2015). Hepatitis B virus polymerase disrupts K63-linked ubiquitination of STING to block innate cytosolic DNA-sensing pathways. Journal of virology *89*, 2287-2300.

Loo, Y.-M., Fornek, J., Crochet, N., Bajwa, G., Perwitasari, O., Martinez-Sobrido, L., Akira, S., Gill, M.A., García-Sastre, A., and Katze, M.G. (2008). Distinct RIG-I and MDA5 signaling by RNA viruses in innate immunity. Journal of virology *82*, 335-345.

Loo, Y.-M., and Gale Jr, M. (2011). Immune signaling by RIG-I-like receptors. Immunity *34*, 680-692.

McCartney, S.A., Thackray, L.B., Gitlin, L., Gilfillan, S., Virgin IV, H.W., and Colonna, M. (2008). MDA-5 recognition of a murine norovirus. PLoS pathogens *4*, e1000108.

Panda, D., Pascual-Garcia, P., Dunagin, M., Tudor, M., Hopkins, K.C., Xu, J., Gold, B., Raj, A., Capelson, M., and Cherry, S. (2014). Nup98 promotes antiviral gene expression to restrict RNA viral infection in Drosophila. Proceedings of the National Academy of Sciences *111*, E3890-E3899.

Pandey, S., Kawai, T., and Akira, S. (2015). Microbial sensing by Toll-like receptors and intracellular nucleic acid sensors. Cold Spring Harbor perspectives in biology *7*, a016246.

Pfaffl, M.W. (2001). A new mathematical model for relative quantification in real-time RT–PCR. Nucleic acids research *29*, e45-e45.

Rabut, G., Doye, V., and Ellenberg, J. (2004). Mapping the dynamic organization of the nuclear pore complex inside single living cells. Nature cell biology *6*, 1114-1121.

Rehwinkel, J., Tan, C.P., Goubau, D., Schulz, O., Pichlmair, A., Bier, K., Robb, N., Vreede, F., Barclay, W., and Fodor, E. (2010). RIG-I detects viral genomic RNA during negative-strand RNA virus infection. Cell *140*, 397-408.

Rothenfusser, S., Goutagny, N., DiPerna, G., Gong, M., Monks, B.G., Schoenemeyer, A., Yamamoto, M., Akira, S., and Fitzgerald, K.A. (2005). The RNA helicase Lgp2 inhibits TLR-independent sensing of viral replication by retinoic acid-inducible gene-I. J Immunol *175*, 5260-5268.

Sachdev, R., Sieverding, C., Flötenmeyer, M., and Antonin, W. (2012). The C-terminal domain of Nup93 is essential for assembly of the structural backbone of nuclear pore complexes. Molecular biology of the cell *23*, 740-749.

Saito, T., Hirai, R., Loo, Y.-M., Owen, D., Johnson, C.L., Sinha, S.C., Akira, S., Fujita, T., and Gale, M. (2007). Regulation of innate antiviral defenses through a shared repressor domain in RIG-I and LGP2. Proceedings of the National Academy of Sciences *104*, 582-587.

Saitoh, T., Fujita, N., Hayashi, T., Takahara, K., Satoh, T., Lee, H., Matsunaga, K., Kageyama, S., Omori, H., and Noda, T. (2009). Atg9a controls dsDNA-driven dynamic translocation of STING and the innate immune response. Proceedings of the National Academy of Sciences *106*, 20842-20846.

Sok, S.P., Ori, D., Nagoor, N.H., and Kawai, T. (2018). Sensing self and non-self DNA by innate immune receptors and their signaling pathways. Critical Reviews™ in Immunology *38*.

Sun, L., Wu, J., Du, F., Chen, X., and Chen, Z.J. (2013). Cyclic GMP-AMP synthase is a cytosolic DNA sensor that activates the type I interferon pathway. Science *339*, 786-791.

Tanaka, Y., and Chen, Z.J. (2012). STING specifies IRF3 phosphorylation by TBK1 in the cytosolic DNA signaling pathway. Sci. Signal. *5*, ra20-ra20.

Thompson, M.R., Kaminski, J.J., Kurt-Jones, E.A., and Fitzgerald, K.A. (2011). Pattern recognition receptors and the innate immune response to viral infection. Viruses *3*, 920-940.

Wang, Q., Liu, X., Cui, Y., Tang, Y., Chen, W., Li, S., Yu, H., Pan, Y., and Wang, C. (2014). The E3 ubiquitin ligase AMFR and INSIG1 bridge the activation of TBK1 kinase by modifying the adaptor STING. Immunity *41*, 919-933.

Xylourgidis, N., Roth, P., Sabri, N., Tsarouhas, V., and Samakovlis, C. (2006). The nucleoporin Nup214 sequesters CRM1 at the nuclear rim and modulates NFκB activation in Drosophila. Journal of cell science *119*, 4409-4419.

Yedavalli, V.S., Neuveut, C., Chi, Y.-h., Kleiman, L., and Jeang, K.-T. (2004). Requirement of DDX3 DEAD box RNA helicase for HIV-1 Rev-RRE export function. Cell *119*, 381-392.

Yoneyama, M., and Fujita, T. (2008). Structural mechanism of RNA recognition by the RIG-I-like receptors. Immunity *29*, 178-181.

Zhang, K., Daigle, J.G., Cunningham, K.M., Coyne, A.N., Ruan, K., Grima, J.C., Bowen, K.E., Wadhwa, H., Yang, P., and Rigo, F. (2018). Stress granule assembly disrupts nucleocytoplasmic transport. Cell *173*, 958-971. e917.